Upscaling for Adiabatic Solid–Fluid Reactions in Porous Medium Using a Volume Averaging Theory

Chen Yang[1,2] · **Michel Quintard**[1,3] · **Gérald Debenest**[1]

Abstract In this paper, an upscaling study of solid–fluid combustion in porous medium with homogeneous and heterogeneous heat sources is carried out using a volume averaging theory. For the sake of simplicity, the reaction rate is assumed to be of first-order Arrhenius type and convection is not taken into account. Local thermal non-equilibrium is considered between the solid and fluid phases. During the resolution of closure problems, periodic boundary condition is utilized in order to determine the effective coefficients in the upscaled model.The obtained macroscale theory is validated against direct numerical simulation results for two typical porous medium geometries made of simple unit cells, namely unconsolidated and consolidated porous media. The comparisons between the present upscaled and microscale results are conducted for various Damköhler numbers for both homogeneous and heterogeneous reaction cases. It has been found that, for the low Damköhler number cases, the temperature profiles generated from the derived upscaled model are in accordance with that of the microscale model. For the high Damköhler number cases, however, the macroscale model fails to predict the combustion front and temperature profile, which evidently suggests that the effects of neglected terms during the upscaling process should be re-examined carefully in further investigations.

Keywords Upscaling · Volume averaging · Thermal non-equilibrium · Damköhler number · Arrhenius reaction rate

✉ Gérald Debenest
debenest@imft.fr

Chen Yang
cyang@imft.fr

Michel Quintard
quintard@imft.fr

1 Institut de Mécanique des Fluides de Toulouse, Université de Toulouse; INPT, UPS; IMFT, Allée Camille Soula, 31400 Toulouse, France

2 School of Chemical Engineering, Fuzhou University, Fuzhou 350116, China

3 CNRS; IMFT, 31400 Toulouse, France

List of Symbols

Latin Symbols

$\mathbf{b}$	Closure variable (m)
$\mathbf{C}$	Closure variable ($\mathrm{W\,m^{-2}\,K^{-1}}$)
$\mathbf{K}$	Effective thermal conductivity tensor ($\mathrm{W\,m^{-1}\,K^{-1}}$)
$\mathbf{n}$	Normal unit vector
$\mathbf{u}$	Transport coefficient ($\mathrm{J\,m^{-2}\,s^{-1}\,K^{-1}}$)
A_0	Pre-exponential factor ($\mathrm{s^{-1}}$)
a_V	Specific surface ($\mathrm{m^{-1}}$)
A_{fm}	Surface area between the fluid and solid phases ($\mathrm{m^2}$)
c_p	Specific heat capacity at constant pressure ($\mathrm{J\,kg^{-1}\,K^{-1}}$)
E	Activation energy ($\mathrm{J\,mol^{-1}}$)
F	Arbitrary function of Taylor series
H	Heat of chemical reaction ($\mathrm{J\,m^{-3}}$)
h	Heat transfer coefficient ($\mathrm{J\,m^{-3}\,s^{-1}\,K^{-1}}$)
k	Thermal conductivity ($\mathrm{W\,m^{-1}\,K^{-1}}$)
L	Macroscopic characteristic length (m)
l	Microscopic characteristic length (m)
q_{rxn}	Heat flux due to the chemical reaction ($\mathrm{W\,m^{-3}}$)
R	Universal gas constant ($\mathrm{J\,mol^{-1}\,K^{-1}}$)
r	Closure variable ($\mathrm{K\,m^2\,s\,J^{-1}}$)
s	Closure variable (s)
T	Temperature (K)
t	Time (s)
V	Unit cell volume ($\mathrm{m^3}$)
x, y	Cartesian coordinates (m)

Greek Symbols

ϵ	Porosity (−)
ρ	Density ($\mathrm{kg\,m^{-3}}$)
τ	Tortuosity (−)
ξ	Distribution coefficient (−)
ζ	Arbitrary function for the closure problem

Subscripts

f	Fluid phase
in	Inlet
int	Interface between the solid and fluid phases
m	Solid phase
rxn	Reaction
u	Unit cell

Superscripts

f	Fluid phase
m	Solid phase

1 Introduction

Coupling between transport phenomena in porous media and reactions appears in many fields of engineering sciences such as bioremediation (Clement et al. 1996), drying (Whitaker 1977), pyrolytic decomposition (Puiroux et al. 2004) or combustion (Akkutlu and Yortsos 2002). Often, transport phenomena are described at one relevant scale: the microscale or the macroscale for instance. Considering combustion problems, for instance, the model may be used at the microscale to check some assumptions (local-scale equilibrium or not as in Debenest et al. 2005) or at the macroscopic or Darcy's scale using effective macroscale parameters (Bruining et al. 2009). How to relate these two scales of description? Developing a proper upscaling procedure is more challenging when the transport equations are coupled with other linear or nonlinear processes such as reactions.

Upscaling transport phenomena in porous media has been the subject of many contributions, and to deal with this fundamental issue, various upscaling methods have been developed. Marle (1967), Slattery (1967) and Whitaker (1967) developed the volume averaging method, whereas Sanchez-Palencia (1980) made use of homogenization techniques and Matheron (1965) used stochastic analysis. The coupling between transport phenomenon and reaction and its upscaling are not novel fields. For instance, Marle (1982) proposed to upscale diffusion and reaction processes in multiphase flow to obtain a macroscale model using the volume averaging theory. A large review has been done in Cushman et al. (2002), and reader could also refer to references herein.

One of the interesting approaches and pioneer works, with an upscaling perspective, on mass transport phenomena and coupled heterogeneous reactions was those of Ryan (1983), Shapiro and Brenner (1986), Whitaker (1987) but also Shapiro and Brenner (1988). Valdés-Parada and Aguilar-Madera (2011) extended this study to linear heterogeneous reactions in porous media. Interesting results were obtained for larger Thiele modulus than the one studied by Ryan (1983) (less than unity). They carried out the upscaling process of mass transport with chemical reaction in porous media using the method of volume averaging under diffusive and dispersive conditions. It has been found that, for the homogeneous chemical reaction case, the effective reaction rate is simply the multiplication of its microscopic counterpart with the porosity, whereas an effective reaction rate coefficient should be obtained from a closure problem for the heterogeneous chemical reaction case. A recent contribution made by Valdés-Parada and Alvarez-Ramirez (2010) is a study on diffusion and homogeneous reaction in porous media. All these studies were carried out in an *isothermal case* and considering linear reactivities regarding concentration. Considering thermal transport in porous media with homogeneous and heterogeneous heat sources, Quintard and Whitaker (1993) and Quintard and Whitaker (2000) developed an upscaling analysis based on the volume averaging theory. In their works, the assumptions of local thermal equilibrium and local thermal non-equilibrium between the solid and fluid phases have been discussed extensively. Nevertheless, the heat source they treated was assumed to be constant and uniform, which is not generally applicable for the case of chemical reaction terms which take generally the form of a highly nonlinear expression of Arrhenius type. As a consequence of the above analysis, we see that

different problems must be resolved when trying to develop macroscale models for heat and mass transfers in porous media with chemical reaction: the problem of local equilibrium or local non-equilibrium, the impact of reaction on dispersion properties, effective reaction rates, and the coupling with heat transfer and highly nonlinear reaction rates. Our objective in this paper is to check the validity and possibly improve the generalized non-equilibrium model proposed by Quintard and Whitaker (2000) taking into account *nonlinear* homogeneous and heterogeneous reaction sources. We limited, however, our ambitions to a chemical reaction simplified to a zeroth-order Arrhenius type, namely the dependency of the reaction term with the reactant concentration was not taken into consideration, but it remains nonlinear with temperature. The absence of concentration dependence is certainly a limitation of the model for many practical applications. However, this limitation allowed us to go more deeply into the question of how to upscale heat transfer problems with highly nonlinear source terms, especially in the case of local non-equilibrium models. A full coupling with dispersion of the various chemical species potentially involved in the reaction will be the objective of future studies.

The emphasis in this paper will be on local non-equilibrium models. Indeed, these models have shown their potential to capture, even in extreme conditions, the local-scale behavior in multiphase reactive systems. Referring to the literature, Kaviany (1991) made an inventory of various situations and defined possible macroscale models to treat phase changes, reaction and transport phenomena in multiphase systems. From this screening study, we see that flow problems involving chemical reactions, such as the case for combustion in multiphase systems, often lead to local non-equilibrium processes and, therefore, requires the development of such theories. Some problems have been formally upscaled in the literature. Sahraoui and Kaviany (1994) proposed averaged models for premixed flames in porous media. Duval et al. (2004) have developed a non-equilibrium model to treat intense evaporation in porous media. Puiroux et al. (2004) developed an original three-phase non-equilibrium model to study heat transfer and pyrolysis in ablative composite layers. In recent studies, Davit et al. (2010a) emphasized the fact that different models may be developed, depending on the interplay of various characteristic time and spatial scales. In particular, they discussed the use of a one-equation *dynamic* model as a substitute for the asymptotic behavior of a more complicated two-equation model. While such a model is simpler and may work under certain conditions (Moyne et al. 2000; Quintard et al. 2001; Davit et al. 2010b), it is not as robust as the two-equation model and may provide wrong indications, as illustrated in Davit and Quintard, (in press). Therefore, we prefer not to develop this model and focus on the classical two-equation model.

In the present study, heat transfer in a porous medium is upscaled with the consideration of homogeneous and heterogeneous source terms, which are assumed to be of the first-order Arrhenius type, i.e., not limited to a mass transport equation but limited by temperature with a nonlinear function. For convenience, we will depict the medium as a two-phase domain with solid inclusions surrounded by a fluid phase. Only conductive transport in the solid and fluid is considered. Local thermal non-equilibrium between the solid and fluid phases is considered. In order to test the theoretical results, microscopic calculations were performed for a simple representation of a porous medium (namely inline arrangement of cylinders), thus allowing for accurate numerical simulations which could be used to compare with macroscale predictions.

2 Upscaling of Purely Conductive Two-Phase Medium

In this section, we will upscale the microscale system of equations in two distinct cases. At first, we will consider the case of a porous medium with homogeneous reaction in the solid

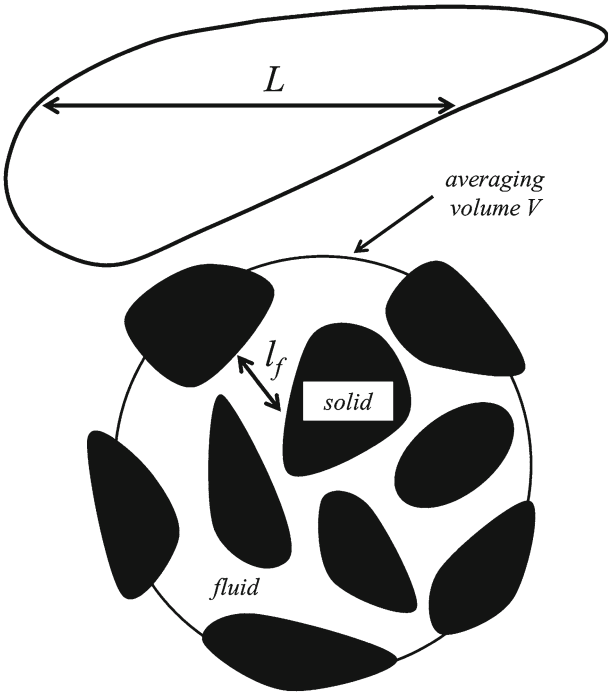

Fig. 1 Averaging volume for solid and fluid phases in the representative elementary volume

phase. Then, we will homogenize the same system in the heterogeneous reaction case where the reaction occurs at the surface between the two phases.

2.1 Pure Conduction with Homogeneous Reaction

We consider a rigid and immobile porous medium saturated by a fluid phase, such as the one sketched in Fig. 1. Subscript f refers to the fluid phase and m to the solid phase.

We are interested in studying heat transport coupled with reactions. As previously mentioned, we first consider the purely conductive case with reactions in the bulk of the solid phase. The reaction rate is a nonlinear function, depending only on the temperature and written using an Arrhenius form, thus providing a strong coupling between heat transport and mass transport. For the solid, energy balance is written as

$$\left(\rho c_p\right)_m \frac{\partial T_m}{\partial t} = \nabla \cdot \left(k_m \nabla T_m\right) + q_{rxn} \tag{1}$$

and for the fluid phase as

$$\left(\rho c_p\right)_f \frac{\partial T_f}{\partial t} = \nabla \cdot \left(k_f \nabla T_f\right) \tag{2}$$

The interfacial boundary conditions are expressed by

$$T_m = T_f \tag{3a}$$

$$\mathbf{n}_{mf} \cdot k_m \nabla T_m = \mathbf{n}_{mf} \cdot k_f \nabla T_f \tag{3b}$$

Furthermore, the reaction rate is assumed to be of zeroth order, so the released heat due to the reaction is

$$q_{rxn} = A_0 e^{-E/RT_m} \times H_{rxn} \tag{4}$$

As indicated above, this reaction rate does not depend on mass concentration. In general, the reaction rate depends on both oxidizer and fuel concentrations. However, in the one-dimensional discrete models, the zeroth-order reactions were widely used as reviewed by Mukasyan and Rogachev (2008). For example, Beeston and Essenhigh (1963) studied the kinetics of coal combustion in vitiated and enriched oxygen atmospheres and pointed out that the reaction rate can be simplified to be zeroth order at a temperature as low as 800 °C. Recently, Vandadi et al. (2013) introduced a novel structure for superadiabatic radiant porous burner to enhance the efficiency. They used the zeroth-order reaction rate to model the combustion fuel and air mixture. It is possible in the case where the reaction is not so dependent of the oxygen concentration. Therefore, we will use the zeroth-order reaction as presented in Eq. (4) to model the combustion in the porous medium in the present study, since our goal is mainly to explore the conditions under which a local thermal non-equilibrium model can be developed for highly nonlinear reactions.

We will now decompose the temperature into two contributions: an average temperature $\langle T_{f,m} \rangle^{f,m}$ and a fluctuation $\widetilde{T}_{f,m}$. One can note the reaction term is only a function of temperature. Using Taylor's series and neglecting the higher terms, for an arbitrary function F, we have

$$F\left(T_{f,m}\right) = F\left(\langle T_{f,m} \rangle^{f,m}\right) + \left(T_{f,m} - \langle T_{f,m} \rangle^{f,m}\right) \left\{ \frac{\partial F}{\partial T_{f,m}} \bigg|_{T_{f,m}=\langle T_{f,m} \rangle^{f,m}} \right. \\ + \frac{1}{2}\left(T_{f,m} - \langle T_{f,m} \rangle^{f,m}\right)^2 \left\{ \frac{\partial^2 F}{\partial T_{f,m}^2} \bigg|_{T_{f,m}=\langle T_{f,m} \rangle^{f,m}} \right. + \cdots \tag{5}$$

Using the decomposition law $T_{f,m} = \langle T_{f,m} \rangle^{f,m} + \widetilde{T}_{f,m}$, we have

$$F\left(T_{f,m}\right) = F\left(\langle T_{f,m} \rangle^{f,m}\right) + \left(\widetilde{T}_{f,m}\right) \left\{ \frac{\partial F}{\partial T_{f,m}} \bigg|_{T_{f,m}=\langle T_{f,m} \rangle^{f,m}} \right. \\ + \frac{1}{2}\left(\widetilde{T}_{f,m}\right)^2 \left\{ \frac{\partial^2 F}{\partial T_{f,m}^2} \bigg|_{T_{f,m}=\langle T_{f,m} \rangle^{f,m}} \right. + \cdots \tag{6}$$

We made the choice to develop Eq. (4) with a Taylor series using the average value of temperature in the REV. Replacing F by the reaction heat equation gives

$$q_{rxn} = A_0 e^{-E/R\langle T_m \rangle^m} \times H_{rxn} + \widetilde{T}_m A_0 H_{rxn} \frac{E}{R\left(\langle T_m \rangle^m\right)^2} e^{-E/R\langle T_m \rangle^m} + \cdots \tag{7}$$

The upscaling process involves many steps which have been discussed at length in the literature. We will not provide details for the most well-known aspects which can be found in Whitaker (1999) for the associated discussion and will focus on the original parts. Macroscale temperatures are defined over the representative elementary volume (Bear 1972) sketched in Fig. 1 as

$$\langle T_m \rangle = \frac{1}{V} \int_{V_m} T_m \mathrm{d}V, \qquad \langle T_m \rangle^m = \frac{1}{V_m} \int_{V_m} T_m \mathrm{d}V \tag{8a}$$

$$\langle T_m \rangle = \epsilon_m \langle T_m \rangle^m \tag{8b}$$

where

$$\epsilon_m = V_m / V \tag{9}$$

In addition, the local phase temperatures are related to the intrinsic phase averages and their corresponding deviations based on Gray's (1975) spatial decomposition written as follows

$$T_m = \langle T_m \rangle^m + \widetilde{T}_m \tag{10a}$$

$$T_f = \langle T_f \rangle^f + \widetilde{T}_f \tag{10b}$$

All subsequent development will make use of the assumption of scale separation, usually expressed as $l_f, l_m \ll r_0 \ll L$.The averaging of Eqs. (1) and (4), after usual modifications involving the classical averaging theorems, leads to

$$\epsilon_m \left(\rho c_p\right)_m \frac{\partial \langle T_m \rangle^m}{\partial t} = \nabla \cdot \left(\epsilon_m k_m \nabla \langle T_m \rangle^m\right) + \nabla \cdot \left(\frac{k_m}{V} \int_{A_{mf}} \mathbf{n}_{mf} \widetilde{T}_m dA\right) + \frac{1}{V} \int_{A_{mf}} \mathbf{n}_{mf} \cdot k_m \nabla T_m dA + \langle q_{rxn} \rangle \tag{11}$$

Dividing Eq. (11) by ϵ_m, which we assume to be constant (Darcy-scale homogeneous medium), one obtains

$$\left(\rho c_p\right)_m \frac{\partial \langle T_m \rangle^m}{\partial t} = \nabla \cdot \left(k_m \nabla \langle T_m \rangle^m\right) + \epsilon_m^{-1} \nabla \cdot \left(\frac{k_m}{V} \int_{A_{mf}} \mathbf{n}_{mf} \widetilde{T}_m \mathrm{d}A\right) + \frac{\epsilon_m^{-1}}{V} \int_{A_{mf}} \mathbf{n}_{mf} \cdot k_m \nabla \widetilde{T}_m \mathrm{d}A + \epsilon_m^{-1} \langle q_{rxn} \rangle \tag{12}$$

With reference to Eq. (7), further manipulation of the last term on the right side gives

$$\begin{aligned} \langle q_{rxn} \rangle &= \frac{1}{V} \int_{V_m} \left(A_0 H_{rxn} + \widetilde{T}_m A_0 H_{rxn} \frac{E}{R \left(\langle T_m \rangle^m\right)^2}\right) e^{-E/R\langle T_m \rangle^m} dV \\ &= \left(\epsilon_m A_0 H_{rxn} + A_0 H_{rxn} \frac{E}{R \left(\langle T_m \rangle^m\right)^2} \langle \widetilde{T}_m \rangle\right) e^{-E/R\langle T_m \rangle^m} \end{aligned} \tag{13}$$

Furthermore, the averaging of Eq. (2) based on the similar procedures presented in the preceding part generates

$$\left(\rho c_p\right)_f \frac{\partial \langle T_f \rangle^f}{\partial t} = \nabla \cdot \left(k_f \nabla \langle T_f \rangle^f\right) + \epsilon_f^{-1} \nabla \cdot \left(\frac{k_f}{V} \int_{A_{fm}} \mathbf{n}_{fm} \widetilde{T}_f dA\right) + \frac{\epsilon_f^{-1}}{V} \int_{A_{fm}} \mathbf{n}_{fm} \cdot k_f \nabla \widetilde{T}_f dA \tag{14}$$

Now applying the decomposition Eqs. (10a) to (1), we obtain

$$\left(\rho c_p\right)_m \frac{\partial \langle T_m \rangle^m}{\partial t} + \left(\rho c_p\right)_m \frac{\partial \widetilde{T}_m}{\partial t} = \nabla \cdot \left(k_m \nabla \langle T_m \rangle^m\right) + \nabla \cdot \left(k_m \nabla \widetilde{T}_m\right) + q_{rxn} \tag{15}$$

Replacing the reaction term in the above equation by Eq. (13) and then subtracting it from Eq. (12), we have the following equation

$$\begin{aligned}\left(\rho c_p\right)_m \frac{\partial \widetilde{T}_m}{\partial t} &= \nabla \cdot \left(k_m \nabla \widetilde{T}_m\right) - \epsilon_m^{-1} \nabla \cdot \left(\frac{k_m}{V} \int_{A_{mf}} \mathbf{n}_{mf} \widetilde{T}_m \mathrm{d}A\right) \\ &- \frac{\epsilon_m^{-1}}{V} \int_{A_{mf}} \mathbf{n}_{mf} \cdot k_m \nabla \widetilde{T}_m dA \\ &- \left(\langle \widetilde{T}_m \rangle \epsilon_m^{-1} - \widetilde{T}_m\right) A_0 H_{rxn} \frac{E}{R\left(\langle T_m \rangle^m\right)^2} e^{-E/R\langle T_m \rangle^m} \end{aligned} \tag{16}$$

It is important to notice that the derivation of Eq. (16) involves neglecting the spatial variations of k_m within V. In addition, under the constraint of length scales separation, it is reasonable to regard intrinsic averaged quantities as linear within the REV so that Eq. (12) is a local equation. In the development of Eq. (16), we made the assumption that the medium is locally homogeneous, in particular, ϵ_m can be extracted from differential operators or integrals. This is most of the time a reasonable assumption, unless one is close to a boundary, problem that requires a specific treatment, or in the case where the medium structure is strongly modified during the combustion process.

We can simplify this result on the basis of the restrictions ($l_m \ll L$)

$$\nabla \cdot \left(k_m \nabla \widetilde{T}_m\right) \gg \epsilon_m^{-1} \nabla \cdot \left(\frac{k_m}{V} \int_{A_{mf}} \mathbf{n}_{mf} \widetilde{T}_m \mathrm{d}A\right) \tag{17}$$

$$\langle \widetilde{T}_m \rangle = 0 \tag{18}$$

Therefore, Eq. (16) can be simplified as follows

$$\left(\rho c_p\right)_m \frac{\partial \widetilde{T}_m}{\partial t} = \nabla \cdot \left(k_m \nabla \widetilde{T}_m\right) - \frac{\epsilon_m^{-1}}{V} \int_{A_{mf}} \mathbf{n}_{mf} \cdot k_m \nabla \widetilde{T}_m \mathrm{d}A + \widetilde{T}_m Da \frac{k_m}{l_m^2} \tag{19}$$

where Da is the Damköhler number defined as follows

$$Da = \frac{H_{rxn}}{(\rho c_p)_m} \frac{E}{R\left(\langle T_m \rangle^m\right)^2} \frac{A_0 e^{-E/R\langle T_m \rangle^m} l_m^2}{k_m/(\rho c_p)_m} \tag{20}$$

The conduction term can be estimated as

$$\nabla \cdot \left(k_m \nabla \widetilde{T}_m\right) = \mathbf{O}\left(\frac{k_m \widetilde{T}_m}{l_m^2}\right) \tag{21}$$

and the estimation of the interfacial flux term is

$$\frac{\epsilon_m^{-1}}{V} \int_{A_{mf}} \mathbf{n}_{mf} \cdot k_m \nabla \widetilde{T}_m \mathrm{d}A = \mathbf{O}\left(\frac{\epsilon_m^{-1} k_m \widetilde{T}_m}{l_m L}\right) \tag{22}$$

In order to compare the significance of the reaction term with the two other terms in Eq. (19), we need to evaluate the multiplier term of $\widetilde{T}_m$ in the last term of this equation. To this end, we consider $\langle T_m \rangle^m$ equal to the combustion front temperature. However, this is not a constant value and varies with time. Referring to some other parameters presented in Table 1, we adopted the coefficients in the reaction schemes proposed by David et al. (2003), who conducted thermal gravimetric analysis on cardboard material at different heating rates. In order to obtain different Damköhler numbers, the pre-exponential factor A_0 varies substantially as shown in Table 1.

Table 1 Parameters for estimation of the reaction term

Parameter	A_0	E	H_{rxn}	k_m	l_m	R
Unit	$1/s$	J/mol	J/m^3	W/m °C	m	J/mol K
Value	$10^5 - 10^8$	6.8×10^4	2.25×10^6	1.5	3×10^{-3}	8.314

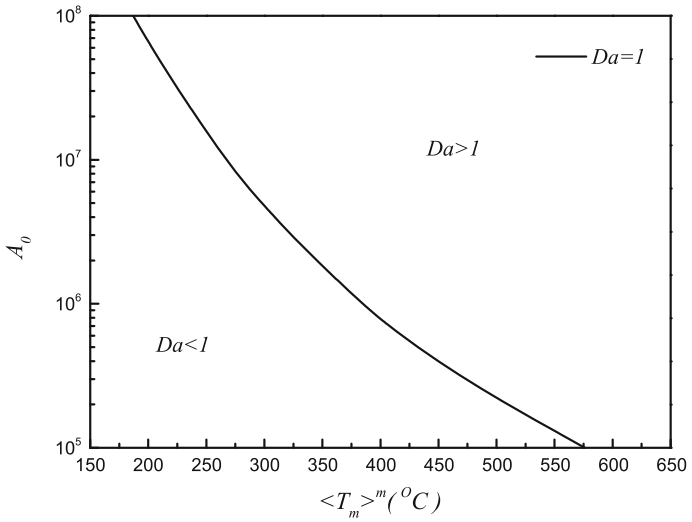

Fig. 2 The value of Damköhler number in Eq. (20) with the variations of $\langle T_m \rangle^m$ and A_0

Based on these values, estimations of the three multiplying terms in the right side of Eq. (19) are

$$\text{conduction term:} \quad \frac{k_m}{l_m^2} \tag{23a}$$

$$\text{interfacial flux term:} \quad \frac{\epsilon_m^{-1} k_m}{l_m L} = \frac{\epsilon_m^{-1} l_m}{L} \frac{k_m}{l_m^2} \ll \frac{k_m}{l_m^2} \tag{23b}$$

$$\text{reaction term:} \quad Da \frac{k_m}{l_m^2} \tag{23c}$$

One should note that the value of $\langle T_m \rangle^m$ plays an important role in this comparison. Fig. 2 indicates how the Damköhler number in Eq. (20) changes with temperature and pre-exponential factor. We may conclude that, for small temperature values, the reaction term becomes negligible, but when the temperature increases, this term becomes dominant by comparison with the conduction and interfacial exchange terms. Based on this figure, we assume that the rightmost term in Eq. (19) is negligible compared to the other terms, only for the case where the Damköhler number defined in Eq. (20) is <1. According to Aldushin et al. (1999), we can obtain an analytical estimate of the characteristic front temperature. Even if heat losses are important, a superadiabatic regime might be observed. Reference temperature depends on the thermal capacities and mass balance of fuel and oxidant. Then, referring to the results of this study, one can obtain an estimate of the multiplier terms.

At the small scale, we can establish the deviation equations for temperature in the two phases. In the solid,

$$\left(\rho c_p\right)_m \frac{\partial \widetilde{T}_m}{\partial t} = \nabla \cdot \left(k_m \nabla \widetilde{T}_m\right) - \frac{\epsilon_m^{-1}}{V} \int_{A_{mf}} \mathbf{n}_{mf} \cdot k_m \nabla \widetilde{T}_m \mathrm{d}A \tag{24}$$

In the fluid,

$$\left(\rho c_p\right)_f \frac{\partial \widetilde{T}_f}{\partial t} = \nabla \cdot \left(k_f \nabla \widetilde{T}_f\right) - \frac{\epsilon_f^{-1}}{V} \int_{A_{mf}} \mathbf{n}_{fm} \cdot k_f \nabla \widetilde{T}_f \mathrm{d}A \tag{25}$$

The interfacial boundary conditions

$$\widetilde{T}_m = \widetilde{T}_f + \left\langle T_f \right\rangle^f - \langle T_m \rangle^m \qquad \text{at } A_{fm} \tag{26a}$$

$$\mathbf{n}_{mf} \cdot k_m \nabla \widetilde{T}_m = \mathbf{n}_{mf} \cdot k_f \nabla \widetilde{T}_f + \mathbf{n}_{mf} \cdot k_f \nabla \left\langle T_f \right\rangle^f - \mathbf{n}_{mf} \cdot k_m \nabla \langle T_m \rangle^m \quad \text{at } A_{fm} \tag{26b}$$

At this point of the development, we have to solve a mixed problem combining the macroscale equations Eqs. (12) and (14) with the microscale equations Eqs. (24) and (25), as well as the boundary conditions Eqs. (26a) and (26b). Such problems have received a lot of attention in the literature, as discussed in Davit et al. (2012). Several models may be built depending on the degree of approximation of the coupling. If one wants to keep the whole dynamic of the coupling, a closure may be introduced involving time convolution products (Moyne 1997; Davit et al. 2012). As shown in Davit et al. (2012), the time convolutions after some relaxation times may be approximated by a quasi-steady closure, which plays a fundamental role in the discussion about the various macroscale models. In this paper, we will use such a closure, and following Quintard and Whitaker (1993), we introduce the following representations for $\widetilde{T}_m$ and $\widetilde{T}_f$.

$$\widetilde{T}_m = \mathbf{b}_{mm} \cdot \nabla \langle T_m \rangle^m + \mathbf{b}_{mf} \cdot \nabla \left\langle T_f \right\rangle^f + s_m \left(\langle T_m \rangle^m - \left\langle T_f \right\rangle^f \right) + \zeta_m \tag{27a}$$

$$\widetilde{T}_f = \mathbf{b}_{fm} \cdot \nabla \langle T_m \rangle^m + \mathbf{b}_{ff} \cdot \nabla \left\langle T_f \right\rangle^f - s_f \left(\left\langle T_f \right\rangle^f - \langle T_m \rangle^m \right) + \zeta_f \tag{27b}$$

where ζ_m and ζ_f are arbitrary functions, and $\mathbf{b}_{mm}$, $\mathbf{b}_{mf}$, $\mathbf{b}_{fm}$, $\mathbf{b}_{ff}$, s_m and s_f are known as the closure variables. The corresponding closure problems can be found in "Appendix 1."

Introducing the representations of Eqs. (27a) and (27b) into the averaged equations Eqs. (12) and (14), we obtain a two-equation model (TEM) with reaction in the solid phase such as

$$\begin{aligned} \epsilon_m \left(\rho c_p\right)_m \frac{\partial \langle T_m \rangle^m}{\partial t} = {} & \nabla \cdot \left(\mathbf{K}_{mm} \cdot \nabla \langle T_m \rangle^m + \mathbf{K}_{mf} \cdot \nabla \left\langle T_f \right\rangle^f \right) + \mathbf{u}_{mm} \cdot \nabla \langle T_m \rangle^m \\ & + \mathbf{u}_{mf} \cdot \nabla \left\langle T_f \right\rangle^f - h \left(\langle T_m \rangle^m - \left\langle T_f \right\rangle^f \right) + \epsilon_m A_0 e^{-E/R\langle T_m \rangle^m} \times H_{rxn} \end{aligned} \tag{28}$$

$$\begin{aligned} \epsilon_f \left(\rho c_p\right)_f \frac{\partial \left\langle T_f \right\rangle^f}{\partial t} = {} & \nabla \cdot \left(\mathbf{K}_{ff} \cdot \nabla \left\langle T_f \right\rangle^f + \mathbf{K}_{fm} \cdot \nabla \langle T_m \rangle^m \right) + \mathbf{u}_{fm} \cdot \nabla \langle T_m \rangle^m \\ & + \mathbf{u}_{ff} \cdot \nabla \left\langle T_f \right\rangle^f + h \left(\langle T_m \rangle^m - \left\langle T_f \right\rangle^f \right) \end{aligned} \tag{29}$$

where the transport coefficients are defined by

$$\mathbf{K}_{mm} = \epsilon_m k_m \mathbf{I} + \frac{k_m}{V} \int_{A_{mf}} \mathbf{n}_{mf} \mathbf{b}_{mm} dA \tag{30a}$$

$$\mathbf{K}_{mf} = \frac{k_m}{V} \int_{A_{mf}} \mathbf{n}_{mf} \mathbf{b}_{mf} dA \tag{30b}$$

$$\mathbf{K}_{ff} = \epsilon_f k_f \mathbf{I} + \frac{k_f}{V} \int_{A_{mf}} \mathbf{n}_{fm} \mathbf{b}_{ff} dA \tag{30c}$$

$$\mathbf{K}_{fm} = \frac{k_f}{V} \int_{A_{mf}} \mathbf{n}_{fm} \mathbf{b}_{fm} dA \tag{30d}$$

The heat transfer coefficient has already been defined in Eq. (71) and is given by the resolution of the closure problem Eqs. (67) through (69). The four non-traditional convective transport terms in Eqs. (28) and (29) depend on the coefficients $\mathbf{u}_{mm}$, $\mathbf{u}_{mf}$, $\mathbf{u}_{fm}$ and $\mathbf{u}_{ff}$ that are determined by

$$\mathbf{u}_{mm} = \frac{1}{V} \int_{A_{mf}} \mathbf{n}_{mf} \cdot k_m \nabla \mathbf{b}_{mm} \mathrm{d}A + \frac{k_m}{V} \int_{A_{mf}} \mathbf{n}_{mf} s_m \mathrm{d}A \tag{31a}$$

$$\mathbf{u}_{mf} = \frac{1}{V} \int_{A_{mf}} \mathbf{n}_{mf} \cdot k_m \nabla \mathbf{b}_{mf} \mathrm{d}A - \frac{k_m}{V} \int_{A_{mf}} \mathbf{n}_{mf} s_m \mathrm{d}A \tag{31b}$$

$$\mathbf{u}_{fm} = \frac{1}{V} \int_{A_{mf}} \mathbf{n}_{fm} \cdot k_f \nabla \mathbf{b}_{fm} \mathrm{d}A + \frac{k_f}{V} \int_{A_{mf}} \mathbf{n}_{fm} s_f \mathrm{d}A \tag{31c}$$

$$\mathbf{u}_{ff} = \frac{1}{V} \int_{A_{mf}} \mathbf{n}_{fm} \cdot k_f \nabla \mathbf{b}_{ff} \mathrm{d}A - \frac{k_f}{V} \int_{A_{mf}} \mathbf{n}_{fm} s_f \mathrm{d}A \tag{31d}$$

As a partial conclusion, we may emphasize the fact that starting with a purely conductive problem, we have obtained a TEM of a conductive form with cross-terms and some additional convective terms. The average flux exchanged between the two phases involves a traditional exchange term with additional "convective"-like terms. Finally, the nonlinear reaction rate is expressed in terms of the average temperature only, but we must keep in mind that there is below this result an assumption that the Da number is small enough. This assumption will be tested later in this paper.

This allows to close the entire macroscale model, and effective parameters calculations will be done in simple unit cells. We will now study the case of heterogeneous Arrhenius reaction between two phases and the local non-equilibrium macroscale model.

2.2 Pure Conduction with Heterogeneous Reaction

We consider now the same porous medium, but the reaction will take place at the interface separating the two phases. We write the system of equations, with adapted boundary conditions, as

$$\left(\rho c_p\right)_m \frac{\partial T_m}{\partial t} = \nabla \cdot \left(k_m \nabla T_m\right) \qquad \text{in } V_m \tag{32}$$

$$\left(\rho c_p\right)_f \frac{\partial T_f}{\partial t} = \nabla \cdot \left(k_f \nabla T_f\right) \qquad \text{in } V_f \tag{33}$$

$$T_{\text{int}} = T_m = T_f \qquad \text{at } A_{fm} \tag{34a}$$

$$\mathbf{n}_{fm} \cdot k_f \nabla T_f = \mathbf{n}_{fm} \cdot k_m \nabla T_m + q_{rxn} \qquad \text{at } A_{fm} \tag{34b}$$

where the heterogeneous reaction heat is taken as

$$q_{rxn} = A_0 e^{-E/RT_{\text{int}}} \times H_{rxn} \tag{35}$$

Here, we keep the same mathematical notation than for the homogeneous reaction for sake of simplicity, while units and values are different. Moreover, the Damköhler number for the heterogeneous reaction case is different with the Eq. (20) and defined as follows

$$Da = \frac{A_0 e^{-E/R\langle T_m\rangle^m} l_m}{k_m/(\rho c_p)_m} \tag{36}$$

Following the volume averaging method outlined before, we can obtain two macroscopic equations

$$\begin{aligned}\epsilon_m \left(\rho c_p\right)_m \frac{\partial \langle T_m\rangle^m}{\partial t} &= \nabla \cdot \left[k_m \left(\epsilon_m \nabla \langle T_m\rangle^m + \frac{1}{V}\int_{A_{mf}} \mathbf{n}_{mf} \widetilde{T}_m \mathrm{d}A\right)\right] \\ &+ \frac{1}{V}\int_{A_{mf}} \mathbf{n}_{mf} \cdot k_m \nabla T_m dA\end{aligned} \tag{37}$$

for the solid, and

$$\begin{aligned}\epsilon_f \left(\rho c_p\right)_f \frac{\partial \left\langle T_f\right\rangle^f}{\partial t} &= \nabla \cdot \left[k_f \left(\epsilon_f \nabla \left\langle T_f\right\rangle^f + \frac{1}{V}\int_{A_{fm}} \mathbf{n}_{fm} \widetilde{T}_f \mathrm{d}A\right)\right] \\ &+ \frac{1}{V}\int_{A_{fm}} \mathbf{n}_{fm} \cdot k_f \nabla T_f dA\end{aligned} \tag{38}$$

for the fluid.

Furthermore, the governing equations of the spatial deviation temperatures are obtained after manipulations similar to the ones outlined in the previous section. We have

$$\left(\rho c_p\right)_m \frac{\partial \widetilde{T}_m}{\partial t} = \nabla \cdot \left(k_m \nabla \widetilde{T}_m\right) - \frac{\epsilon_m^{-1}}{V}\int_{A_{mf}} \mathbf{n}_{mf} \cdot k_m \nabla \widetilde{T}_m \mathrm{d}A \qquad \text{in } V_m \tag{39}$$

and

$$\left(\rho c_p\right)_f \frac{\partial \widetilde{T}_f}{\partial t} = \nabla \cdot \left(k_f \nabla \widetilde{T}_f\right) - \frac{\epsilon_f^{-1}}{V}\int_{A_{fm}} \mathbf{n}_{fm} \cdot k_f \nabla \widetilde{T}_f \mathrm{d}A \qquad \text{in } V_f \tag{40}$$

The interfacial boundary conditions give

$$\widetilde{T}_m = \widetilde{T}_f + \left\langle T_f\right\rangle^f - \langle T_m\rangle^m \qquad \text{at } A_{fm} \tag{41a}$$

$$\begin{aligned}\mathbf{n}_{fm} \cdot k_f \nabla \widetilde{T}_f &= \mathbf{n}_{fm} \cdot k_m \nabla \widetilde{T}_m - \mathbf{n}_{fm} \cdot k_f \nabla \left\langle T_f\right\rangle^f \\ &+ \mathbf{n}_{fm} \cdot k_m \nabla \langle T_m\rangle^m + q_{rxn}\end{aligned} \tag{41b}$$

Analogous to Eq. (7), the heterogeneous reaction heat can also be expanded as the function of $\left\langle T_f\right\rangle^f$ and $\widetilde{T}_f$. Then, one can have

$$q_{rxn} = A_0 e^{-E/R\left\langle T_f\right\rangle^f} \times H_{rxn} + \widetilde{T}_f A_0 H_{rxn} \frac{E}{R\left(\left\langle T_f\right\rangle^f\right)^2} e^{-E/R\left\langle T_f\right\rangle^f} + \cdots \tag{42}$$

Based on the boundary condition Eq. (41a), the combination of Eqs. (7) and (42) readily gives spatial deviation temperature of solid phase at the interface:

$$\begin{aligned}\widetilde{T}_m &= \frac{\frac{E}{R\left(\langle T_f\rangle^f\right)^2}e^{-E/R\langle T_f\rangle^f}\left(\langle T_m\rangle^m-\langle T_f\rangle^f\right)-\left(e^{-E/R\langle T_m\rangle^m}-e^{-E/R\langle T_f\rangle^f}\right)}{\frac{E}{R\left(\langle T_m\rangle^m\right)^2}e^{-E/R\langle T_m\rangle^m}-\frac{E}{R\left(\langle T_f\rangle^f\right)^2}e^{-E/R\langle T_f\rangle^f}}\\ &= w\end{aligned} \tag{43}$$

In this study, following the discussion in the previous section, the closure problem is assumed to be quasi-steady. As a consequence, the closure problem can be simplified to

$$0=\nabla\cdot\left(k_m\nabla\widetilde{T}_m\right)-\frac{\epsilon_m^{-1}}{V}\int_{A_{mf}}\mathbf{n}_{mf}\cdot k_m\nabla\widetilde{T}_m\mathrm{d}A \tag{44}$$

$$0=\nabla\cdot\left(k_f\nabla\widetilde{T}_f\right)-\frac{\epsilon_f^{-1}}{V}\int_{A_{fm}}\mathbf{n}_{fm}\cdot k_f\nabla\widetilde{T}_f\mathrm{d}A \tag{45}$$

Based on the flux boundary condition Eq. (41b), these two surface integrals can be related by

$$\frac{1}{V}\int_{A_{fm}}\mathbf{n}_{fm}\cdot k_f\nabla\widetilde{T}_f\mathrm{d}A=\frac{1}{V}\int_{A_{fm}}\mathbf{n}_{fm}\cdot k_m\nabla\widetilde{T}_m\mathrm{d}A+a_V\langle q_{rxn}\rangle_{fm} \tag{46}$$

where

$$\begin{aligned}\langle q_{rxn}\rangle_{fm} &= \frac{1}{A_{fm}}\int_{A_{fm}}\left(A_0H_{rxn}+wA_0H_{rxn}\frac{E}{R\left(\langle T_m\rangle^m\right)^2}\right)e^{-E/R\langle T_m\rangle^m}dA\\ &= \left(1+w\frac{E}{R\left(\langle T_m\rangle^m\right)^2}\right)A_0H_{rxn}e^{-E/R\langle T_m\rangle^m}\end{aligned} \tag{47}$$

According to Quintard and Whitaker (1993, 2000), this form of the closure problem suggests the following representations for $\widetilde{T}_m$ and $\widetilde{T}_f$.

$$\widetilde{T}_m=\mathbf{b}_{mm}\cdot\nabla\langle T_m\rangle^m+\mathbf{b}_{mf}\cdot\nabla\langle T_f\rangle^f+s_m\left(\langle T_m\rangle^m-\langle T_f\rangle^f\right)+r_m\langle q_{rxn}\rangle_{fm} \tag{48a}$$

$$\widetilde{T}_f=\mathbf{b}_{fm}\cdot\nabla\langle T_m\rangle^m+\mathbf{b}_{ff}\cdot\nabla\langle T_f\rangle^f-s_f\left(\langle T_f\rangle^f-\langle T_m\rangle^m\right)+r_f\langle q_{rxn}\rangle_{fm} \tag{48b}$$

where r_m and r_f are the specific closure variables for the heterogeneous case. The closure variables $\mathbf{b}_{mm}$, $\mathbf{b}_{mf}$, $\mathbf{b}_{fm}$, $\mathbf{b}_{ff}$, s_m and s_f can be solved by the Eqs. (57)–(71). Therefore, the focus in this part is to determine how the heterogeneous heat source is distributed between the solid and the fluid. This is the major difference with the preceding section. As the reaction occurs at the local scale on the surface A_{fm}, the macroscale distribution of heat is not given a priori. The problem of the impact of the heat source terms has received less attention, but our idea is to follow the development presented in Quintard and Whitaker (2000). The corresponding closure problem takes the form

$$k_m\nabla^2r_m=a_V\epsilon_m^{-1}\xi_m\qquad\text{in } V_m \tag{49}$$

Boundary conditions

$$r_f=r_m\qquad\text{at } A_{fm} \tag{50a}$$

$$\mathbf{n}_{fm}\cdot k_f\nabla r_f=\mathbf{n}_{fm}\cdot k_m\nabla r_m+1\qquad\text{at } A_{fm} \tag{50b}$$

$$k_f \nabla^2 r_f = a_V \epsilon_f^{-1} \xi_f \qquad \text{in } V_f \tag{51}$$

$$\text{Periodicity:} \quad r_f(\mathbf{r} + \ell_i) = r_f(\mathbf{r}), \qquad r_m(\mathbf{r} + \ell_i) = r_m(\mathbf{r}), \qquad i = 1, 2, 3 \tag{52a}$$

$$\text{Average:} \quad \langle r_f \rangle^f = 0, \qquad \langle r_m \rangle^m = 0 \tag{52b}$$

where ξ_m and ξ_f are given by

$$\xi_m = \frac{1}{A_{mf}} \int_{A_{mf}} \mathbf{n}_{mf} \cdot k_m \nabla r_m dA, \quad \xi_f = \frac{1}{A_{fm}} \int_{A_{fm}} \mathbf{n}_{fm} \cdot k_f \nabla r_f dA \tag{53}$$

According to the boundary condition Eq. (50b), we get

$$\xi_f + \xi_m = 1 \tag{54}$$

After determining the terms associated with the spatial deviation temperatures, we can obtain the closed form of the macroscopic governing equations given by

$$\begin{aligned} \epsilon_m (\rho c_p)_m \frac{\partial \langle T_m \rangle^m}{\partial t} &= \nabla \cdot \left(\mathbf{K}_{mm} \nabla \langle T_m \rangle^m + \mathbf{K}_{mf} \nabla \langle T_f \rangle^f \right) + \mathbf{u}_{mm} \cdot \nabla \langle T_m \rangle^m \\ &+ \mathbf{u}_{mf} \cdot \nabla \langle T_f \rangle^f - h \left(\langle T_m \rangle^m - \langle T_f \rangle^f \right) \\ &+ a_V \xi_m \left(1 + w \frac{E}{R \left(\langle T_m \rangle^m \right)^2} \right) A_0 e^{-E/R \langle T_m \rangle^m} H_{rxn} \end{aligned} \tag{55}$$

for the macroscale solid phase and

$$\begin{aligned} \epsilon_f (\rho c_p)_f \frac{\partial \langle T_f \rangle^f}{\partial t} &= \nabla \cdot \left(\mathbf{K}_{ff} \nabla \langle T_f \rangle^f + \mathbf{K}_{fm} \nabla \langle T_m \rangle^m \right) + \mathbf{u}_{fm} \cdot \nabla \langle T_m \rangle^m \\ &+ \mathbf{u}_{ff} \cdot \nabla \langle T_f \rangle^f + h \left(\langle T_m \rangle^m - \langle T_f \rangle^f \right) \\ &+ a_V \xi_f \left(1 + w \frac{E}{R \left(\langle T_m \rangle^m \right)^2} \right) A_0 e^{-E/R \langle T_m \rangle^m} H_{rxn} \end{aligned} \tag{56}$$

for the macroscale fluid phase.

In this section, the two macroscale models associated with the homogeneous and heterogeneous reactions are obtained. The appearance of these two models are similar, but the corresponding two thermal sources play different roles in the closure problem. As pointed out by Quintard and Whitaker (2000), the heterogeneous thermal source gives rise to both a source and a coupling term, whereas the homogeneous thermal source gives rise to only a coupling term.

3 Physical Model and Validations

In this section, we are interested in validation tests. Even if one would normally use complex unit cells and more realistic geometries for practical applications, we will only use simple unit cells, which have all the necessary characteristics for the testing purposes. Those are illustrated in Fig. 3. The first one is typical of an unconsolidated porous medium, in which the cylinders are placed in inline arrangement. In addition, the second one is an example of consolidated porous medium, in which the solid matrix is connected and surrounded by the

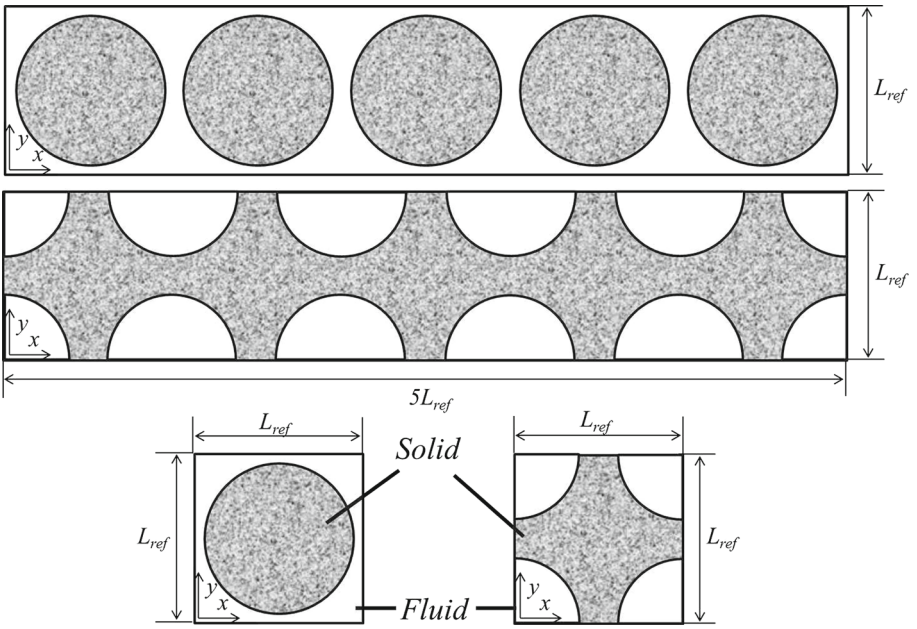

Fig. 3 Schematic of the *DNS* models and the unit cells

quadrant voids. This latter case was chosen because we know that contact point effects may have a strong impact for heat transfer problem (Shonnard and Whitaker 1989; Davarzani et al. 2011). As shown in the previous part, there are closure variables which need to be determined in the upscaled model. Generally, the closure calculations are carried out by using symmetric unit cells (Ryan et al. 1981; Eidsath et al. 1983; Ochoa et al. 1986; Kim et al. 1987; Quintard 1993) for illustrating effective properties behavior. Moreover, Nozad et al. (1985) claimed that the utilization of periodic boundary condition in the closure problem can provide excellent agreement between theory and experiment for disordered systems.

While the use of periodic boundary condition is fulfilled in our case given the geometry periodicity, we would like to remind the reader that, in many real cases, the use of periodic conditions is impossible. With the development of imaging techniques like X-ray tomography, it is possible to access the 3D microstructure of porous media. In some cases, the traditional periodic closure problem may be used to give an acceptable estimate of the effective properties, but the periodicity conditions may result in dramatic errors according to the results of Lux (2010). Comparing the use of different boundary conditions to determine the effective diffusion tensor of low porosity materials, he showed how bad could be the estimate when using periodic conditions, due to percolation effects.

In this study, the first geometry will be used in order to check the accuracy of our upscaling method by comparison with previous works. The second one is different and was chosen in order to investigate the effects of contact between solids. It must be noticed that this is not a realistic geometry in terms of transport in the "fluid" phase, which is now not percolating, but it serves our purposes to emphasize the impact of a continuous solid phase.

Based on those unit cells, closure variables are calculated and the corresponding effective properties are presented in Figs. 4, 5, 6 and 7. In order to validate the upscaled model, the properties calculated from the first unit cell are compared with that of Quintard et al. (1997). The integro-differential system of equations is solved using the COMSOL Multiphysics

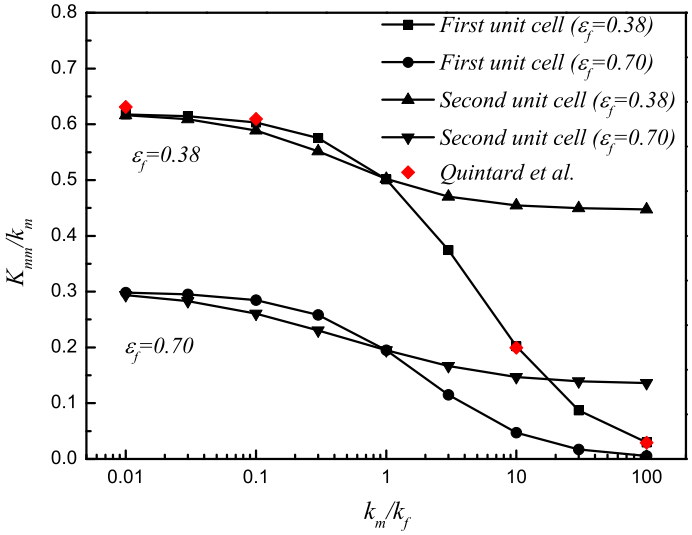

Fig. 4 Effective conductivity of the macroscale solid phase versus the ratio k_m/k_f and for different porosities

package. For the convergence criteria, the residuals of all equations are $< 10^{-6}$. Moreover, we have performed a sensitivity analysis to the grid size, which can guarantee that all of the calculation results in this study are independent of the grid size with a relative error $< 2\,\%$. In all cases, the results of our calculations are compared with the one of Quintard et al. (1997) for the first unit cell, namely the inline arrangement of cylinders. For two porosities equal to 0.38 and 0.70, results in Figs. 4, 5, 6 and 7 show a very good agreement between our calculations and those previously obtained based on a finite volume method over a Cartesian grid.

In Figs. 4, 5, 6 and 7, the effects of contact between solids on the effective properties of porous medium are addressed. Furthermore, the effects of porosity on the effective properties of porous medium based on the two unit cells are also investigated in these four figures.

In Fig. 4, the effective solid conductivity is plotted over a large range of small-scale conductivity ratio. With the rise of k_m/k_f, the effective conductivity $\mathbf{K}_{mm}/k_m = K_{mm}/k_m\mathbf{I}$ decreases and approaches a constant value, depending on the porosity and unit cell geometry. Based on the analysis conducted in "Appendix 2," K_{mm}/k_m tends to ϵ_m/τ_m in the limit of large ratio k_m/k_f. Here, τ_m is the solid phase tortuosity, which is larger than unity and can be determined by the solution of the closure problem over a representative unit cell. Comparing these two unit cells, it can be seen that effects of contact points are not significant at small ratio k_m/k_f, for the same porosity.

In Fig. 5, the effective fluid phase conductivity is plotted for the two unit cells and two porosities. At a given porosity, it can be clearly seen that the effective conductivity $\mathbf{K}_{ff}/k_f = K_{ff}/k_f\mathbf{I}$ is influenced by the geometry and contact points. At low ratio k_m/k_f, the effective conductivity of the fluid phase based on the second unit cell is zero, because the fluid phase is isolated by the solid phase with low thermal conductivity and not conducting directly the heat within the sample. Same effects are present in the first unit cell, but they are not so important regarding the effective fluid conductivity values determined at low ratio. Based on the analysis conducted in "Appendix 2," K_{ff}/k_f tends to ϵ_f/τ_f in the limit of small ratio k_m/k_f, where τ_f is the fluid phase tortuosity. Moreover, $\mathbf{K}_{ff}/k_f$ is not significantly dependent on the ratio values for the first unit cell. Also, we can note the influence of the porosity on the conductivity values. Increasing the porosity, i.e., increasing the fluid fraction

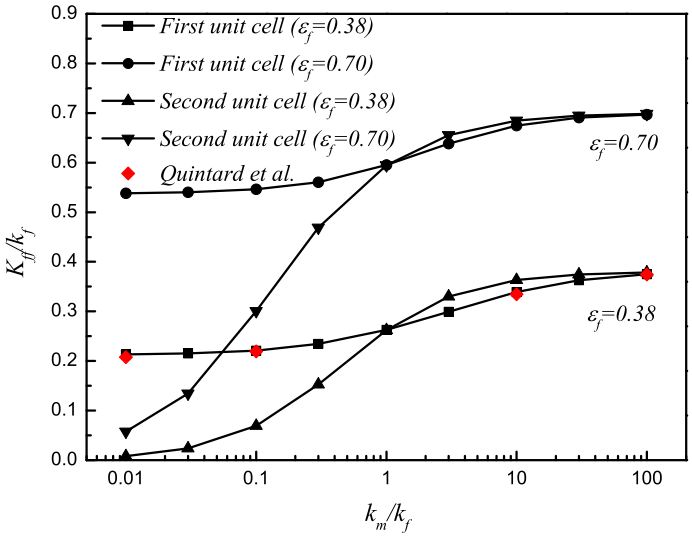

Fig. 5 Effective conductivity of the macroscale fluid phase versus the ratio k_m/k_f and for different porosities

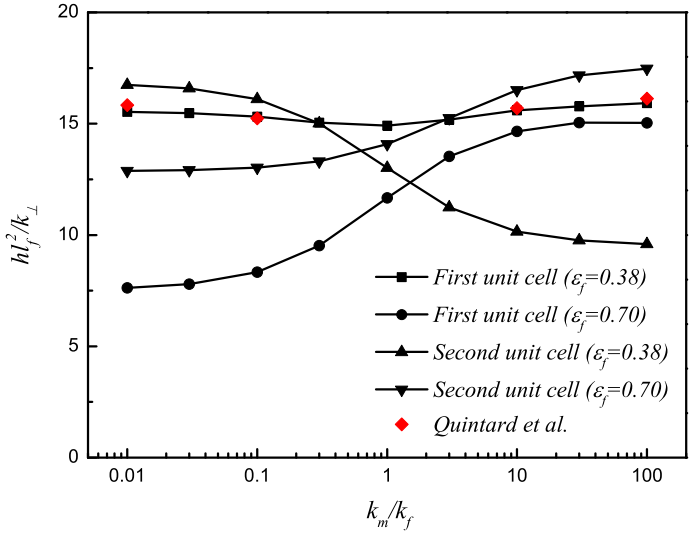

Fig. 6 Heat transfer coefficient for two porous medium geometries and different porosities depending on the ratio k_m/k_f

volume, leads to larger values of $\mathbf{K}_{ff}/k_f$, as expected from the contribution of terms like $\epsilon_\alpha k_\alpha$ in the RHS of Eq. (79). For all cases, with large values of k_m/k_f, a constant value $\mathbf{K}_{ff}/k_f$ is obtained, which is consistent with the previous observations in Quintard and Whitaker (1993). It can be noticed that large ratio values of effective conductivities are the same in all cases, and they do not depend on the geometry at the microscale if the fluid phase is not insulated by solid inclusions.

In Fig. 6, we plot the heat transfer coefficient for two unit cells as a function of the ratio k_m/k_f. It should be mentioned that the parameter $k_\perp$ indicated in Fig. 6 is defined as $\frac{1}{k_\perp} =$

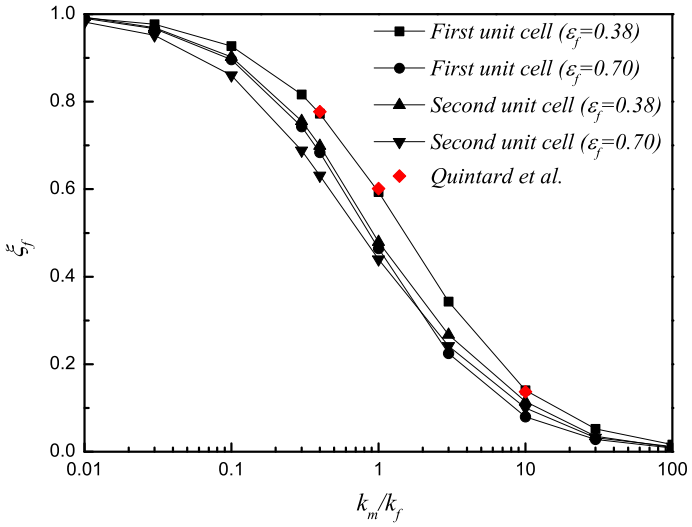

Fig. 7 Distribution coefficient for two porous medium geometries and different porosities depending on the ratio k_m/k_f

$\frac{\epsilon_f}{k_f} + \frac{\epsilon_m}{k_m}$, which is the theoretical lower bound of the effective stagnant thermal conductivity based on the perpendicular model. For the large conductivity ratio, the behaviors of closure problem associated with heat transfer coefficient are investigated in "Appendix 2." The analytical solutions show that the asymptotic behaviors exist when the limit of k_m/k_f (or k_f/k_m) goes to infinity. This phenomenon is consistent with the numerical results observed in Fig. 6.

In Fig. 7, the distribution coefficient is plotted for increasing ratio k_m/k_f. Two porosities and the contact point effects are investigated. At low values of k_m/k_f, all the heat is distributed in the fluid phase. When the heat conduction in the fluid phase is not the dominating process, the distribution coefficient is nearly equal to zero, i.e., all the heat is transferred to the solid phase. This is in good agreement with previous observations made in Quintard et al. (2000). It also can be found that the increase of ϵ_f results in the decrease of the distribution coefficient, but the thermal conductivity ratio k_m/k_f has more significant influence on the distribution coefficient than porosity does for both unit cells.

From the comparisons in these four figures, it can be concluded that for the same porosity, effective conductivities of solid and fluid phases and heat transfer coefficient have a higher dependence on the phase connectivity than the distribution coefficient does. In all cases, we have validated our approach using the comparison with previous calculations from Quintard et al. (1997), Quintard and Whitaker (2000) and then studied the effects of porosity variations and contact points.

4 Validation Against *DNS* Results

In this part, the idea is to verify whether or not the proposed upscaled model is able to reproduce the results obtained with direct numerical simulation (*DNS*) over the microscopic geometry. The system presented in Fig. 3 is under thermal adiabatic condition, except at the inlet face (i.e., $x = 0$) which is kept at a uniform temperature. The main characteristics of

Table 2 Model parameters

Parameter	Value
Unit cell dimension, mm (x, y)	3, 3
Solid dimension for the first unit cell, mm (radius)	1.332
Fluid dimension for the second unit cell, mm (radius)	1.043
Model dimension, mm (x, y)	15, 3
Inlet temperature/Initial temperature (°C)	300/25
Thermal conductivity ratio $\left(\mathrm{k}_m / k_f\right)$	10
Heat capacity ratio $\left(\rho c_p\right)_m / \left(\rho c_p\right)_f$	1.6×10^3

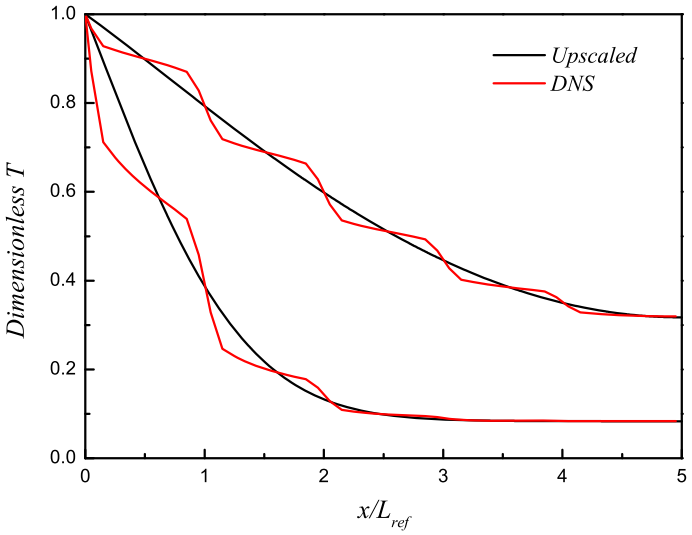

Fig. 8 Low Damköhler number ($Da = 0.2$) for the homogeneous case ($\epsilon_f = 0.38$) based on the first unit cell

the model are given in Table 2. We give the real values used in our calculations and geometry definitions. One can note that we focus our attention on specific values of thermal conductivity and heat capacity ratio close to values encountered in solid–gas combustion (Debenest *et al.* 2005). Furthermore, the dimensionless microscopic and macroscopic governing equations are obtained and presented in "Appendix 3." It should be mentioned that the Damköhler number discussed in this section is based on the inlet temperature and varies by changing the pre-exponential factor A_0.

In Figs. 8, 10 and 12, the comparisons between the upscaled and *DNS* results for the homogeneous case are presented for three different Damköhler numbers and for the first unit cell, namely the inline arrangement of cylinders versus the dimensionless T, which is the ratio of volume averaged temperature to the inlet temperature. In Figs. 9, 11 and 13, we represent the averaged temperature profiles of the upscaled model for the second unit cell at different front locations compared with that of *DNS* model for different Damköhler numbers. In Figs. 8 and 9, for low Damköhler numbers, we obtain a good prediction for the temperature profiles compared to those given using the *DNS* model. Temperature fluctuations are observed for the

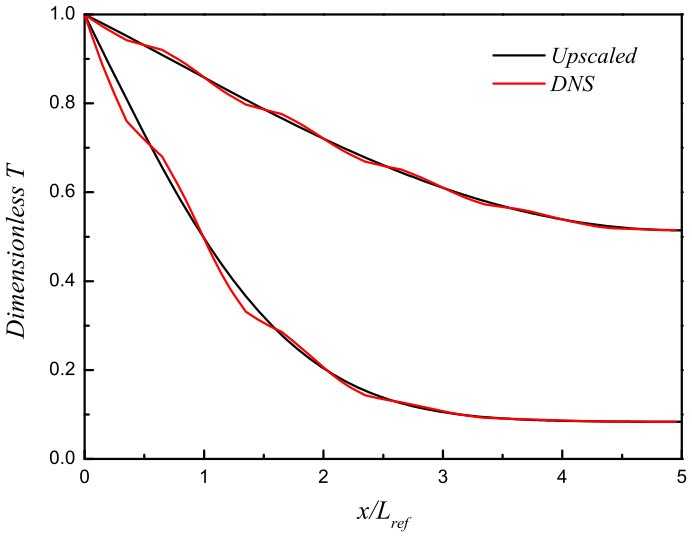

Fig. 9 Low Damköhler number($Da = 0.2$) for the homogeneous case ($\epsilon_f = 0.38$) based on the second unit cell

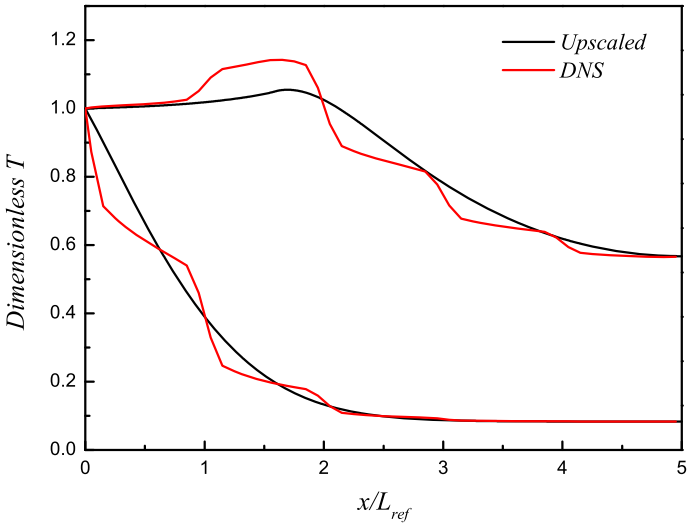

Fig. 10 Medium Damköhler number ($Da = 2$) for the homogeneous case ($\epsilon_f = 0.38$) based on the first unit cell

averaged temperatures in the inline arrangement of cylinders and not so evident in the second unit cell. This is a classical behavior when averaged values are built from the *DNS* results by averaging over a single unit cell. This kind of averaging is not sufficient to produce a completely regularized average field as pointed out by Marle (1965; 1967; 1982), Mls (1987) and Prat (1989). It has been discussed at length in Quintard and Whitaker (1993, 1994a, b, c). This is why we can observe local-scale fluctuations for the *DNS* averaged values in Figs. 8, 10 and 12. However, these values are enough to materialize the trend and permit a comparison with the upscaled model results.

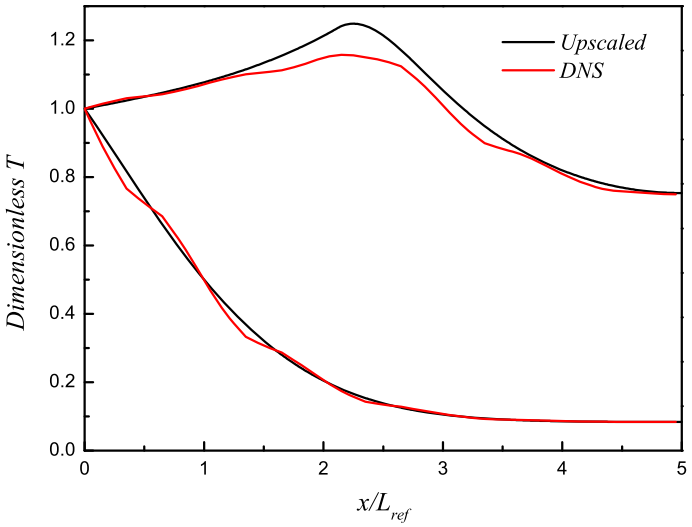

Fig. 11 Medium Damköhler number ($Da = 2$) for the homogeneous case ($\epsilon_f = 0.38$) based on the second unit cell

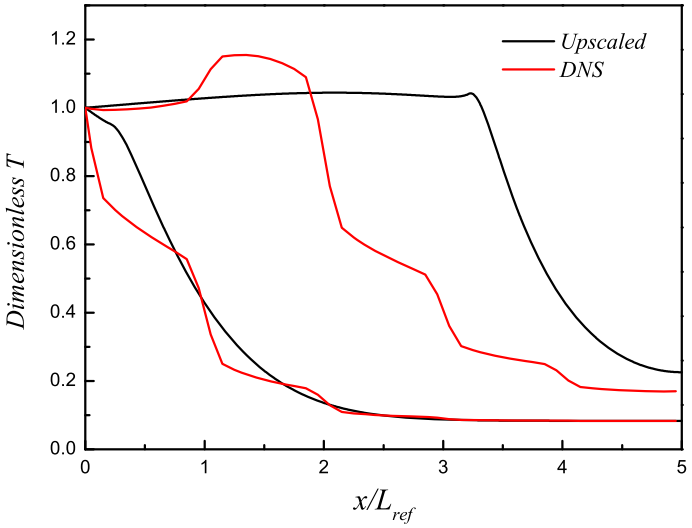

Fig. 12 High Damköhler number ($Da = 20$) for the homogeneous case ($\epsilon_f = 0.38$) based on the first unit cell

For the medium Damköhler number as shown in Figs. 10 and 11, the prediction of the upscaled model is still acceptable at the initial times of the combustion process, where the temperature is not so high. But, after one unit cell, the temperature increases and the upscaled models fail in predicting with accuracy the temperature level. Nevertheless, the differences remain acceptable.

Furthermore, for the high Damköhler number as indicated in Figs. 12 and 13, the upscaled model fails in predicting the temperature. This is because, for high Damköhler number, the rightmost term in Eq. (16) neglected in the present upscaled model becomes significant and

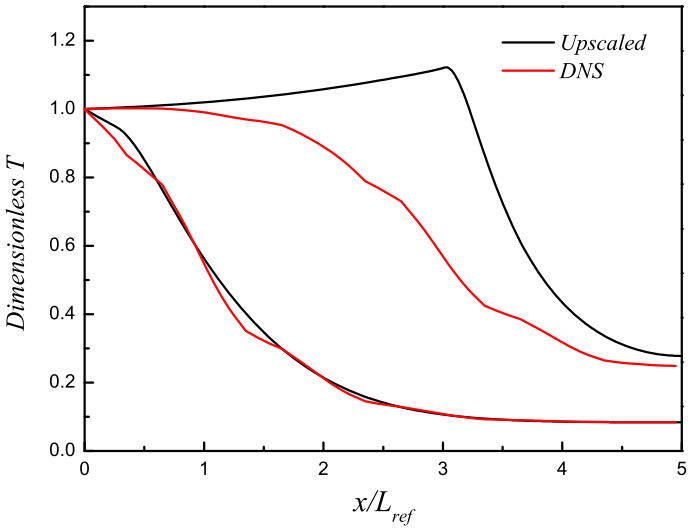

Fig. 13 High Damköhler number ($Da = 20$) for the homogeneous case ($\epsilon_f = 0.38$) based on the second unit cell

more important than the two other terms. Hence, the ignorance of reaction term in Eq. (16) would result in significant discrepancies in this situation. Another possible reason is the discard of higher order terms for the reaction heat term in Eq. (6). Contact point effects are significant in terms of fluctuations within the unit cell when averaging *DNS* results in all cases. They decrease the local-scale variations of temperature. It is important to notice that even with contact point effects, no important differences exist between *DNS* and upscaled model.

In Figs. 8, 9, 10, 11, 12 and 13, it also can be found that for low Damköhler number, no peaks are present in the averaged temperature profiles. These are exactly the same behaviors with those observed in Fadaei (2009). This can be explained by the Damköhler value, where characteristic times for reaction and transport are compared. In this case, $Da = 0.2$, heat is much faster conveyed by conduction than produced by the reaction. Then, no accumulation is possible.

In summary, there are two potential possibilities to further improve the validity of the upscaled model for high Damköhler number:

1. the reconsideration of reaction term in Eq. (16);
2. the utilization of higher order terms in Eq. (6), which would introduce some other closure variables.

The results for the heterogeneous case based on the upscaled and *DNS* models are presented for the two unit cells in Figs. 14, 15, 16, 17, 18 and 19. Once again, for low Damköhler number, in Figs. 14 and 15, the good match between *DNS* results and upscaled approach is obvious. Nevertheless, fluctuations appear more significant with the inline arrangement of cylinders. It is consistent with previous observations for the homogeneous reaction. Even for high Damköhler numbers, the agreement between upscaled approach and the *DNS* results can be considered to be acceptable. In the first unit cell, the same observations are done for fluctuations, but the profiles in the second unit cell are smoother and follow with accuracy the prediction of local-scale model.

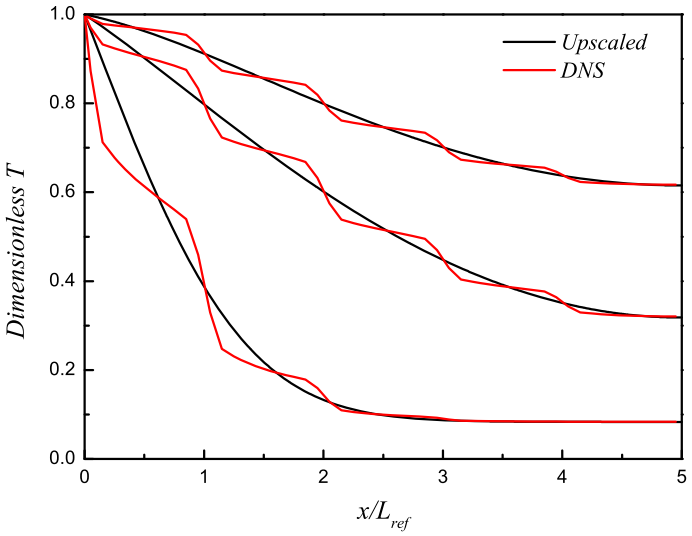

Fig. 14 Low Damköhler number ($Da = 0.2$) for the heterogeneous case ($\epsilon_f = 0.38$) based on the first unit cell

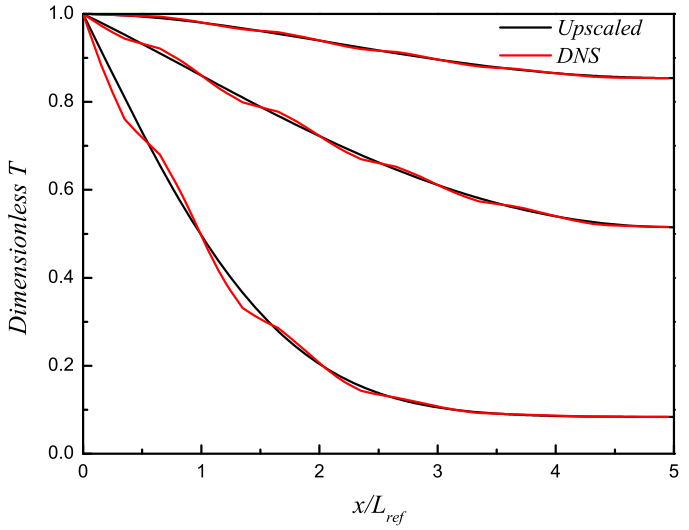

Fig. 15 Low Damköhler number ($Da = 0.2$) for the heterogeneous case ($\epsilon_f = 0.38$) based on the second unit cell

However, with the increase of Damköhler number, the prediction based on the upscaled model is getting worse, especially in the range of high temperature. This suggests to take into account other terms inside the developments of the effective reaction rate. Increasing the reactivity will lead us to strong variations of temperature within the unit cell, and an average value of temperature to estimate the reactivity will lead to major errors.

As discussed in this section, it also should be noted that for both unit cells studied in this paper, the discrepancy between *DNS* and the upscaled model is smaller for the heterogeneous case than that for the homogeneous case. The possible reason is that, for the homogeneous case, the multiplier term of $\widetilde{T}_m$ in the rightmost term of Eq. (19) was neglected for the sake of

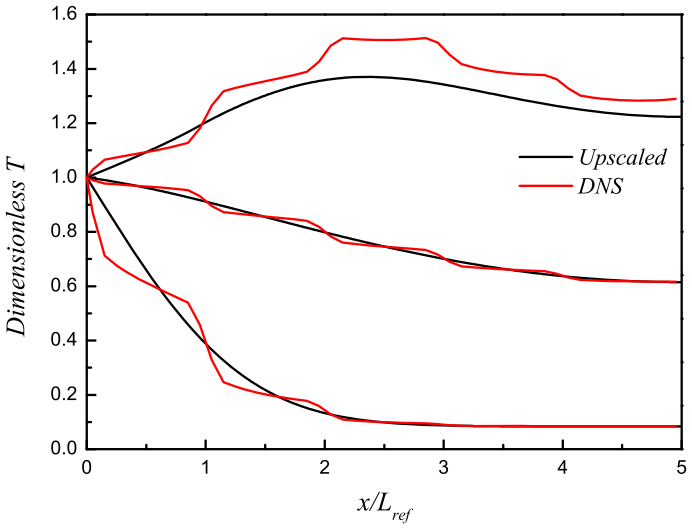

Fig. 16 Medium Damköhler number ($Da = 2$) for the heterogeneous case ($\epsilon_f = 0.38$) based on the first unit cell

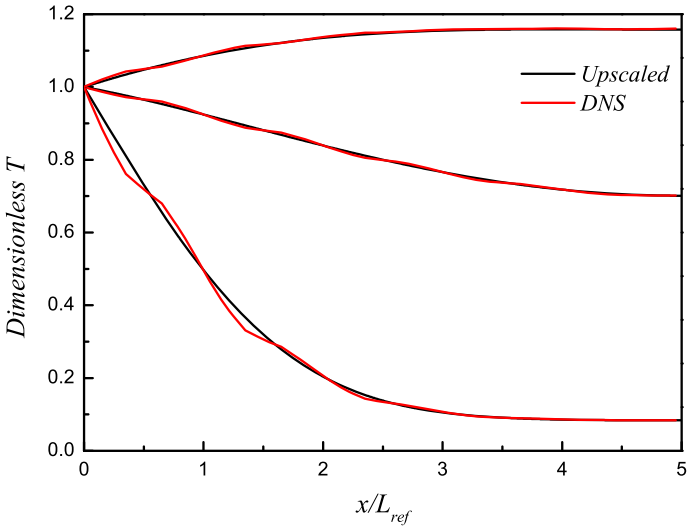

Fig. 17 Medium Damköhler number ($Da = 2$) for the heterogeneous case ($\epsilon_f = 0.38$) based on the second unit cell

simplicity. But this simplification is only suitable for low Da number. For the heterogeneous case, however, the spatial deviation temperature of the solid phase at the interface $\widetilde{T}_m$ was estimated by Eq. (43), which resulted in a better agreement between *DNS* and the upscaled model.

Finally, it should be remarked that our results show that the additional convective-like terms do not play a significant role for the purely diffusive case under consideration and for the 1D initial boundary value problems solved in this paper. For instance, numerical results for the macroscale equations with or without these terms do not exhibit a significant difference.

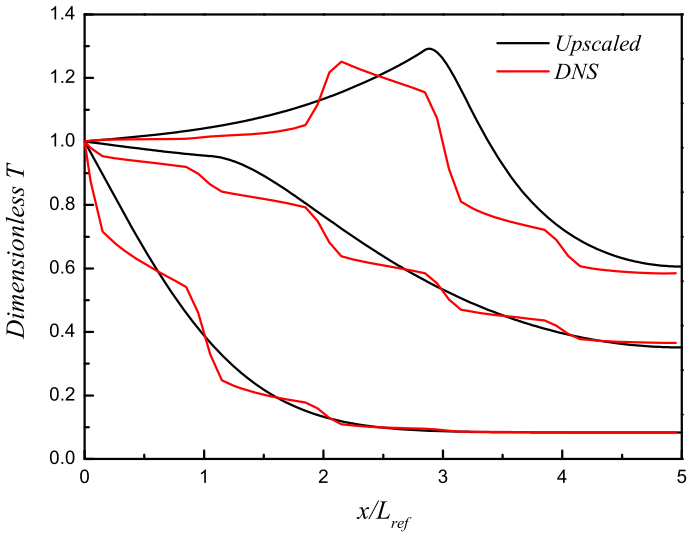

Fig. 18 High Damköhler number ($Da = 20$) for the heterogeneous case ($\epsilon_f = 0.38$) based on the first unit cell

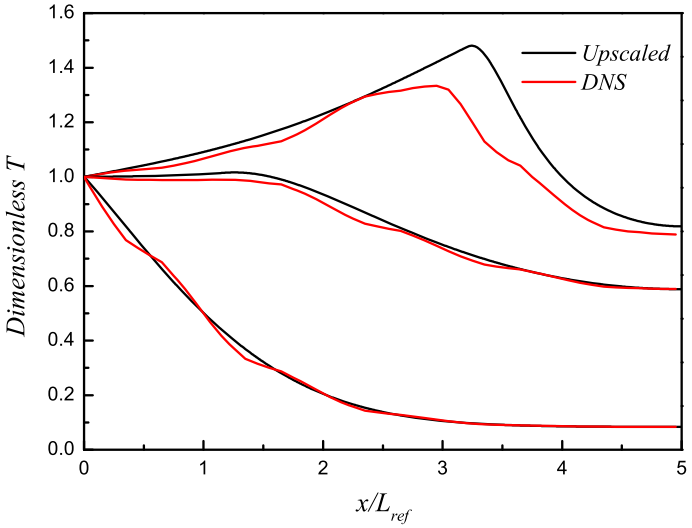

Fig. 19 High Damköhler number ($Da = 20$) for the heterogeneous case ($\epsilon_f = 0.38$) based on the second unit cell

5 Conclusions

In the present study, we have developed a macroscale model for heat transport with Arrhenius type reactions in porous medium. We used a simplified form of the chemical reaction to describe both homogeneous and heterogeneous reactions. The chemical reaction was simplified to be of zeroth-order Arrhenius type, namely the dependency of reactant concentration was not taken into consideration, but it remains nonlinear with temperature. The absence

of concentration dependence is certainly a limitation of the model. However, this limitation allowed us to go more deeply into the question of how to upscale heat transfer problems with highly nonlinear source terms, especially in the case of local non-equilibrium models. A full coupling with dispersion for the various chemical species potentially involved will be the objective of future studies. Moreover, convection at the local scale in the fluid phase was discarded, and local thermal non-equilibrium assumption between the fluid and solid phases was considered, according to the literature review. Based on two unit cell models, we have obtained the effective properties, effective conductivities of each phases, heat transfer coefficient, as well as the distribution coefficient depending on the ratio of conductivities at the local scale. We have compared our values with those of previous studies, in order to validate our approach. The effects of porosity variations were investigated using these two unit cells. At this point, we can make two remarks:

- All the effective parameters depend on the porosity. But the distribution coefficient has much smaller dependence on porosity than other effective properties do.
- The asymptotic behaviors of effective thermal conductivities of solid and fluid phases are investigated analytically and numerically. The effective thermal conductivity ratio of solid phase K_{mm}/k_m approaches to ϵ_m/τ_m in the limit $k_m/k_f \longrightarrow +\infty$, whereas the fluid phase effective thermal conductivity ratio K_{ff}/k_f tends to ϵ_f/τ_f in the limit $k_f/k_m \longrightarrow +\infty$.

In a second time, a comparison between the unconsolidated and consolidated porous medium was made, so as to investigate the effects of contact between solid particles on the effective properties. This is not really significant on the distribution coefficient, but more important for the heat transfer coefficient and effective conductivities. Validity tests were performed by comparing results obtained with the macroscale model and results obtained with direct numerical simulations of the pore-scale equations. We can draw several remarks :

- At low and medium Damköhler numbers, the comparison between local-scale simulations and our macroscale model is good for both homogeneous and heterogeneous reactions (see Figs. 8, 9, 10, 11, 14, 15, 16 and 17), which is consistent with the approximation made in the upscaling process,
- For high Damköhler numbers, the homogeneous reaction case is not well captured by the effective model. The upscaled model is still capable of predicting the location of the combustion front for a medium Damköhler number, whereas it fails to estimate accurately the combustion front temperature. This is mainly due to the rightmost term in Eq. (16) we have ignored in our developments. This is not so evident in the heterogeneous reaction case where local-scale approach is well matched by the effective model for the same range of Damköhler numbers.

This implies that the neglected terms should be re-examined carefully in order to break the bottleneck of the present upscaled model in the range of high Damköhler numbers. One possibility is to keep in the upscaling process the higher order terms, especially those associated with the treatment of the heat sources. This will lead to more complete closure problems and effective properties. Another possibility is the implementation of a mixed model, i.e., the coupling between a macroscale equation, for instance for describing transport in the fluid phase, and a microscale equation in the other phase, for example, the solid phase. This mixed model will be reminiscent to the one of Golfier et al. (2007). The other advantage of this method could be a correct treatment of the Arrhenius function, treated in its original form at the local scale without any linearization process.

Acknowledgments The authors would like to express the sincerest thanks to the financial support funded by ANR-11-BS009-005-01.

Appendix 1: Closure Problems

Here, we followed the same manipulations conducted by Quintard and Whitaker (1993) except that, in our upscaled equation, we have an extra reaction term for the solid phase. The closure variables, defined in Eqs. (27a) and (27b), are introduced in Eqs. (24) and (25) and for these equations to be satisfied at the leading order in terms of $\langle T_m \rangle^m$, $\langle T_f \rangle^f$, $\nabla \langle T_m \rangle^m$ and $\nabla \langle T_f \rangle^f$, they must satisfy the closure problems discussed below.

In the next step, we only need to determine these variables in some representative region in order to evaluate the terms in macroscopic equations that contain the spatial deviation variables. The first closure problem is associated with $\nabla \langle T_m \rangle^m$ and takes the following form.

$$k_m \nabla^2 \mathbf{b}_{mm} = \epsilon_m^{-1} \mathbf{C}_{mm} \qquad \text{in the solid} \tag{57}$$

$$\mathbf{b}_{mm} = \mathbf{b}_{fm} \qquad \text{at } A_{fm} \tag{58a}$$

$$\mathbf{n}_{mf} \cdot k_m \nabla \mathbf{b}_{mm} = \mathbf{n}_{mf} \cdot k_f \nabla \mathbf{b}_{fm} - \mathbf{n}_{mf} k_m \qquad \text{at } A_{fm} \tag{58b}$$

$$0 = k_f \nabla^2 \mathbf{b}_{fm} + \epsilon_f^{-1} \mathbf{C}_{mm} \qquad \text{in the fluid} \tag{59}$$

$$\text{Periodicity:} \quad \mathbf{b}_{fm}(\mathbf{r} + \ell_i) = \mathbf{b}_{fm}(\mathbf{r}), \qquad \mathbf{b}_{mm}(\mathbf{r} + \ell_i) = \mathbf{b}_{mm}(\mathbf{r}), \qquad i = 1, 2, 3 \tag{60a}$$

$$\text{Average:} \quad \langle \mathbf{b}_{fm} \rangle^f = 0, \qquad \langle \mathbf{b}_{mm} \rangle^m = 0 \tag{60b}$$

Here, $\mathbf{C}_{mm}$ is the unknown integral represented by

$$\mathbf{C}_{mm} = \frac{1}{V} \int_{A_{mf}} \mathbf{n}_{mf} \cdot k_m \nabla \mathbf{b}_{mm} dA = \frac{1}{V} \int_{A_{mf}} \mathbf{n}_{mf} \cdot k_f \nabla \mathbf{b}_{fm} dA \tag{61}$$

A detailed description of the evaluation of this unknown integral is given by Quintard et al. (1997).

The term $\nabla \langle T_f \rangle^f$ is also a source in the closure problem for $\widetilde{T}_m$ and $\widetilde{T}_f$. The boundary value problem associated with the closure variable for $\nabla \langle T_f \rangle^f$ is given by

$$k_m \nabla^2 \mathbf{b}_{mf} = \epsilon_m^{-1} \mathbf{C}_{mf} \qquad \text{in the solid} \tag{62}$$

$$\mathbf{b}_{mf} = \mathbf{b}_{ff} \qquad \text{at } A_{fm} \tag{63a}$$

$$\mathbf{n}_{mf} \cdot k_m \nabla \mathbf{b}_{mf} = \mathbf{n}_{mf} \cdot k_f \nabla \mathbf{b}_{ff} + \mathbf{n}_{mf} k_f \qquad \text{at } A_{fm} \tag{63b}$$

$$0 = k_f \nabla^2 \mathbf{b}_{ff} + \epsilon_f^{-1} \mathbf{C}_{mf} \qquad \text{in the fluid} \tag{64}$$

$$\text{Periodicity:} \quad \mathbf{b}_{ff}(\mathbf{r} + \ell_i) = \mathbf{b}_{ff}(\mathbf{r}), \qquad \mathbf{b}_{mf}(\mathbf{r} + \ell_i) = \mathbf{b}_{mf}(\mathbf{r}), \qquad i = 1, 2, 3 \tag{65a}$$

$$\text{Average:} \quad \langle \mathbf{b}_{ff} \rangle^f = 0, \qquad \langle \mathbf{b}_{mf} \rangle^m = 0 \tag{65b}$$

Here, $\mathbf{C}_{mf}$ is the unknown integral represented by

$$\mathbf{C}_{mf} = \frac{1}{V}\int_{A_{mf}} \mathbf{n}_{mf} \cdot k_m \nabla \mathbf{b}_{mf} dA = \frac{1}{V}\int_{A_{mf}} \mathbf{n}_{mf} \cdot k_f \nabla \mathbf{b}_{ff} dA \tag{66}$$

Moving on to the source represented by $\langle T_f \rangle^f - \langle T_m \rangle^m$ in Eq. (26a), we construct the following boundary problem for the closure scalars s_m and s_f.

$$0 = k_m \nabla^2 s_m + \epsilon_m^{-1} h \qquad \text{in the solid} \tag{67}$$

$$s_f = s_m + 1 \qquad \text{at } A_{fm} \tag{68a}$$

$$\mathbf{n}_{mf} \cdot k_m \nabla s_m = \mathbf{n}_{mf} \cdot k_f \nabla s_f \qquad \text{at } A_{fm} \tag{68b}$$

$$0 = k_f \nabla^2 s_f - \epsilon_f^{-1} h \qquad \text{in the fluid} \tag{69}$$

$$\text{Periodicity:} \quad s_f(\mathbf{r} + \ell_i) = s_f(\mathbf{r}), \qquad s_m(\mathbf{r} + \ell_i) = s_m(\mathbf{r}), \qquad i = 1, 2, 3 \tag{70a}$$

$$\text{Average:} \quad \langle s_f \rangle^f = 0, \qquad \langle s_m \rangle^m = 0 \tag{70b}$$

In this closure problem, the undetermined constant is represented by

$$h = \frac{1}{V}\int_{A_{mf}} \mathbf{n}_{fm} \cdot k_m \nabla s_m dA = \frac{1}{V}\int_{A_{mf}} \mathbf{n}_{fm} \cdot k_f \nabla s_f dA \tag{71}$$

Appendix 2: Large Conductivity Ratio Behavior of the Closure Problems

In this appendix, we are interested in the behavior of the closure problems in the limit of k_m/k_f (or k_f/k_m) going to infinity. The results are clear for the mapping variables and the distribution coefficient as illustrated in Fig. 7.

For the closure problem involving the mapping variable s_m and s_f, we have by looking at the limit of Eqs. (67) through (71) when $k_m/k_f \to +\infty$:

$$s_m = 0 \tag{72}$$

and

$$\frac{h l_f^2}{k_f} = constant \tag{73}$$

Similarly, when $k_f/k_m \to +\infty$, we have

$$s_f = 0 \tag{74}$$

and,

$$\frac{h l_f^2}{k_m} = \text{constant} \tag{75}$$

This simply gives the obvious physical result that the heat transfer resistance is due to the less conductive material in these limiting cases.

For the closure problems involving the $\mathbf{b}_{\alpha\beta}$ mapping variables, we can develop the following estimates. Eqs. (57) through (61) lead to in the limit $k_m/k_f \to +\infty$:

$$\mathbf{b}_{mm} = 0 \qquad \text{in } V_m \tag{76}$$

$$\mathbf{n}_{mf} \cdot k_f \nabla \mathbf{b}_{mm} = -\mathbf{n}_{mf} \qquad \text{at } A_{fm} \tag{77}$$

$$\text{Periodicity:} \quad \mathbf{b}_{mm}(\mathbf{r} + \ell_i) = \mathbf{b}_{mm}(\mathbf{r}), \qquad i = 1, 2, 3 \tag{78a}$$

$$\text{Average:} \quad \langle \mathbf{b}_{mm} \rangle^m = 0 \tag{78b}$$

which is the typical effective diffusion problem for the m-phase. Its solution gives for a percolating m-phase, and in the isotropic case:

$$\mathbf{K}_{mm} = \epsilon_m k_m \mathbf{I} + \frac{k_m}{V} \int_{A_{mf}} \mathbf{n}_{mf} \mathbf{b}_{mm} dA = \frac{\epsilon_m k_m}{\tau_m} \mathbf{I} \tag{79}$$

where τ_m is the tortuosity given by the solution of the closure problem over a representative unit cell.

Similarly, in the case $k_f/k_m \to +\infty$, we obtain by looking at Eqs. (62) through (66)

$$\mathbf{K}_{ff} = \epsilon_f k_f \mathbf{I} + \frac{k_f}{V} \int_{A_{mf}} \mathbf{n}_{mf} \mathbf{b}_{ff} dA = \frac{\epsilon_f k_f}{\tau_f} \mathbf{I} \tag{80}$$

where this time τ_f is the calculated tortuosity of the percolating isotropic f-phase.

Appendix 3: Normalization of Governing Equations

In this appendix, the microscale and macroscale governing equations for both homogeneous and heterogeneous reactions presented in this paper are normalized. Firstly, the dimensionless governing equations for homogeneous reaction are written as:

$$\frac{\partial T_m^*}{\partial t^*} = \nabla^2 T_m^* + \frac{Da}{E/RT_{\text{in}}} e^{-\frac{E}{RT_{\text{in}}}\left(\frac{1}{T_m^*} - 1\right)} \tag{81}$$

and

$$\frac{\partial T_f^*}{\partial t^*} \frac{(\rho c_p)_f / k_f}{(\rho c_p)_m / k_m} = \nabla^2 T_f^* \tag{82}$$

The interfacial boundary condition is expressed by

$$T_m^* = T_f^* \tag{83a}$$

$$\mathbf{n}_{mf} \cdot \frac{k_m}{k_f} \nabla T_m^* = \mathbf{n}_{mf} \cdot \nabla T_f^* \tag{83b}$$

where

$$T_m^* = T_m/T_{\text{in}}, \qquad T_f^* = T_f/T_{\text{in}}, \qquad t^* = t\left(k_m/(\rho c_p)_m\right)/L_{\text{ref}}^2 \tag{84a}$$

$$Da = \frac{H_{rxn}}{(\rho c_p)_m} \frac{E}{RT_{\text{in}}^2} \frac{A_0 e^{-E/RT_{\text{in}}} L_{\text{ref}}^2}{k_m/(\rho c_p)_m} \tag{84b}$$

The corresponding dimensionless macroscopic governing equations based on Eqs. (28) and (29) are written as:

$$\begin{aligned}\epsilon_m \frac{\partial \left\langle T_m^* \right\rangle^m}{\partial t^*} &= \nabla \cdot \left(\mathbf{K}_{mm}^* \cdot \nabla \left\langle T_m^* \right\rangle^m + \mathbf{K}_{mf}^* \cdot \nabla \left\langle T_f^* \right\rangle^f \right) + \mathbf{u}_{mm}^* \cdot \nabla \left\langle T_m^* \right\rangle^m \\ &\quad + \mathbf{u}_{mf}^* \cdot \nabla \left\langle T_f^* \right\rangle^f - h^* \left(\left\langle T_m^* \right\rangle^m - \left\langle T_f^* \right\rangle^f \right) \\ &\quad + \epsilon_m \frac{Da}{E/RT_{\text{in}}} e^{-\frac{E}{RT_{\text{in}}} \left(\frac{1}{\langle T_m^* \rangle^m} - 1 \right)} \end{aligned} \tag{85}$$

$$\begin{aligned}\epsilon_f \frac{\left(\rho c_p\right)_f / k_f}{\left(\rho c_p\right)_m / k_m} \frac{\partial \left\langle T_f^* \right\rangle^f}{\partial t^*} &= \nabla \cdot \left(\mathbf{K}_{ff}^* \cdot \nabla \left\langle T_f^* \right\rangle^f + \mathbf{K}_{fm}^* \cdot \nabla \left\langle T_m^* \right\rangle^m \right) \\ &\quad + \mathbf{u}_{fm}^* \cdot \nabla \left\langle T_m^* \right\rangle^m + \mathbf{u}_{ff}^* \cdot \nabla \left\langle T_f^* \right\rangle^f + h^* \frac{k_m}{k_f} \left(\left\langle T_m^* \right\rangle^m - \left\langle T_f^* \right\rangle^f \right) \end{aligned} \tag{86}$$

where

$$\left\langle T_m^* \right\rangle^m = \langle T_m \rangle^m / T_{\text{in}}, \quad \left\langle T_f^* \right\rangle^f = \langle T_f \rangle^f / T_{\text{in}}, \quad \mathbf{K}_{mm}^* = \mathbf{K}_{mm} / k_m \tag{87a}$$

$$\mathbf{K}_{mf}^* = \mathbf{K}_{mf} / k_m, \quad \mathbf{K}_{ff}^* = \mathbf{K}_{ff} / k_f, \quad \mathbf{K}_{fm}^* = \mathbf{K}_{fm} / k_f \tag{87b}$$

$$\mathbf{u}_{mm}^* = \mathbf{u}_{mm} L_{\text{ref}} / k_m, \quad \mathbf{u}_{mf}^* = \mathbf{u}_{mf} L_{\text{ref}} / k_m, \quad \mathbf{u}_{fm}^* = \mathbf{u}_{fm} L_{\text{ref}} / k_f \tag{87c}$$

$$\mathbf{u}_{ff}^* = \mathbf{u}_{ff} L_{\text{ref}} / k_f, \qquad h^* = h L_{\text{ref}}^2 / k_m \tag{87d}$$

Based on the parameters given in Eq. (84a), the dimensionless microscopic governing equations for heterogeneous reaction are obtained as follows:

$$\frac{\partial T_m^*}{\partial t^*} = \nabla^2 T_m^* \qquad \text{in } V_m \tag{88}$$

and

$$\frac{\partial T_f^*}{\partial t^*} \frac{\left(\rho c_p\right)_f / k_f}{\left(\rho c_p\right)_m / k_m} = \nabla^2 T_f^* \qquad \text{in } V_f \tag{89}$$

The adapted boundary conditions are written as

$$T_m^* = T_f^* \qquad \text{at } A_{fm} \tag{90a}$$

$$\mathbf{n}_{fm} \cdot \frac{k_f}{k_m} \nabla T_f^* = \mathbf{n}_{fm} \cdot \nabla T_m^* + Da \frac{H_{rxn}}{\left(\rho c_p\right)_m T_{\text{in}}} e^{-\frac{E}{RT_{\text{in}}} \left(\frac{1}{T_m^*} - 1 \right)} \quad \text{at } A_{fm} \tag{90b}$$

where the Damköhler number for heterogeneous reaction in this paper is different with Eq. (84b) and defined as below

$$Da = \frac{A_0 e^{-E/RT_{\text{in}}} L_{\text{ref}}}{k_m / (\rho c_p)_m} \tag{91}$$

Moreover, we can use Eqs. (87a)–(87d) to normalize Eqs. (55) and (56) and obtain the following dimensionless macroscopic governing equations:

$$\begin{aligned}\epsilon_m \frac{\partial \left\langle T_m^* \right\rangle^m}{\partial t^*} &= \nabla \cdot \left(\mathbf{K}_{mm}^* \cdot \nabla \left\langle T_m^* \right\rangle^m + \mathbf{K}_{mf}^* \cdot \nabla \left\langle T_f^* \right\rangle^f \right) + \mathbf{u}_{mm}^* \cdot \nabla \left\langle T_m^* \right\rangle^m \\ &+ \mathbf{u}_{mf}^* \cdot \nabla \left\langle T_f^* \right\rangle^f - h^* \left(\left\langle T_m^* \right\rangle^m - \left\langle T_f^* \right\rangle^f \right) \\ &+ a_V L_{\text{ref}} \xi_m \left(1 + w^* \frac{E}{RT_{\text{in}} \left(\left\langle T_m^* \right\rangle^m \right)^2} \right) Da \frac{H_{rxn}}{\left(\rho c_p\right)_m T_{\text{in}}} e^{-\frac{E}{RT_{\text{in}}} \left(\frac{1}{\left\langle T_m^* \right\rangle^m} - 1 \right)} \end{aligned} \tag{92}$$

$$\begin{aligned}\epsilon_f \frac{\left(\rho c_p\right)_f / k_f}{\left(\rho c_p\right)_m / k_m} \frac{\partial \left\langle T_f^* \right\rangle^f}{\partial t^*} &= \nabla \cdot \left(\mathbf{K}_{ff}^* \cdot \nabla \left\langle T_f^* \right\rangle^f + \mathbf{K}_{fm}^* \cdot \nabla \left\langle T_m^* \right\rangle^m \right) \\ &+ \mathbf{u}_{fm}^* \cdot \nabla \left\langle T_m^* \right\rangle^m + \mathbf{u}_{ff}^* \cdot \nabla \left\langle T_f^* \right\rangle^f + h^* \frac{k_m}{k_f} \left(\left\langle T_m^* \right\rangle^m - \left\langle T_f^* \right\rangle^f \right) \\ &+ a_V L_{\text{ref}} \xi_f \left(1 + w^* \frac{E}{RT_{\text{in}} \left(\left\langle T_m^* \right\rangle^m \right)^2} \right) Da \frac{H_{rxn}}{\left(\rho c_p\right)_m T_{\text{in}}} e^{-\frac{E}{RT_{\text{in}}} \left(\frac{1}{\left\langle T_m^* \right\rangle^m} - 1 \right)} \end{aligned} \tag{93}$$

where the spatial deviation dimensionless temperature of solid phase at the interface is given by

$$\begin{aligned} w^* &= w / T_{\text{in}} \\ &= \frac{\frac{E}{RT_{\text{in}} \left(\left\langle T_f^* \right\rangle^f \right)^2} e^{\frac{E}{RT_{\text{in}} \left\langle T_f^* \right\rangle^f}} \left(\left\langle T_m^* \right\rangle^m - \left\langle T_f^* \right\rangle^f \right) - \left(e^{\frac{E}{RT_{\text{in}} \left\langle T_m^* \right\rangle^m}} - e^{\frac{E}{RT_{\text{in}} \left\langle T_f^* \right\rangle^f}} \right)}{\frac{E}{RT_{\text{in}} \left(\left\langle T_m^* \right\rangle^m \right)^2} e^{\frac{E}{RT_{\text{in}} \left\langle T_m^* \right\rangle^m}} - \frac{E}{RT_{\text{in}} \left(\left\langle T_f^* \right\rangle^f \right)^2} e^{\frac{E}{RT_{\text{in}} \left\langle T_f^* \right\rangle^f}}} \end{aligned} \tag{94}$$

References

Akkutlu, I.Y., Yortsos, Y.C.: The effect of heterogeneity on in-situ combustion: the propagation of combustion fronts in layered porous media. SPE J. **54**, 56–56 (2002)

Aldushin, A., Rumanov, I., Matkowsky, B.: Maximal energy accumulation in a superadiabatic filtration combustion wave. Combust. Flame **118**, 76–90 (1999)

Bear, J.: Dynamics of Fluids in Porous Media. American Elsevier, New York (1972)

Beeston, G., Essenhigh, R.H.: Kinetics of coal combustion: the influence of oxygen concentration on the burning-out times of single particles. J. Phys. Chem. **67**, 1349–1355 (1963)

Bruining, J., Mailybaev, A.A., Marchesin, D.: Filtration combustion in wet porous medium. SIAM J. Appl. Math. **70**, 1157–1177 (2009)

Clement, T.P., Hooker, B.S., Skeen, R.S.: Macroscopic models for predicting changes in saturated porous media properties caused by microbial growth. Groundwater **34**(5), 934–942 (1996)

Cushman, J.H., Bennethus, L.S., Hu, B.X.: A primer on upscaling tools for porous media. Adv. Water Resour. **25**, 10431067 (2002)

Davarzani, H., Marcoux, M., Quintard, M.: Effect of solid thermal conductivity and particle–particle contact on effective thermodiffusion coefficient in porous media. Int. J. Thermal Sci. **50**, 2328–2339 (2011)

David, C., Salvador, S., Dirion, J.L., Quintard, M.: Determination of a reaction scheme for cardboard thermal degradation using thermal gravimetric analysis. J. Anal. Appl. Pyrolysis **67**, 307–323 (2003)

Davit Y., Quintard, M.: Theoretical analysis of transport in porous media: Multi-Equation and Hybrid Models for a Generic Transport Problem with Non-Linear Source Terms, chapter in press in Handbook of Porous Media, 3rd edition, Ed. By K. Vafai, Taylor & Francis
Davit, Y., Debenest, G., Wood, B.D., Quintard, M.: Modeling non-equilibrium mass transport in biologically reactive porous media. Adv. Water Resour. **33**, 1075–1093 (2010a)
Davit, Y., Quintard, M., Debenest, G.: Equivalence between volume averaging and moments matching techniques for mass transport in porous media. Int. J. Heat Mass Transf. **53**, 4985–4993 (2010b)
Davit, Y., Wood, B.D., Debenest, G., Quintard, M.: Correspondence between one-and two-equation models for solute transport in two-region heterogeneous porous media. Transp. Porous Media **95**, 213–228 (2012)
Debenest, G., Mourzenko, V.V., Thovert, J.F.: Smouldering in fixed beds of oil shale grains: governing parameters and global regimes. Combust. Theory Model. **9**, 301–321 (2005)
Duval, F., Fichot, F., Quintard, M.: A local thermal non-equilibrium model for two-phase flows with phase-change in porous media. Int. J. Heat Mass Transf. **47**, 613–639 (2004)
Eidsath, A., Carbonell, R.G., Whitaker, S., Herrmann, L.R.: Dispersion in pulsed systemsIII: comparison between theory and experiments for packed beds. Chem. Eng. Sci. **38**, 1803–1816 (1983)
Fadaei H.: Etude de la récupération de bruts lourds en réservoir carbonaté fracturé par le procédé de combustion in situ, PhD Thesis, INP Toulouse (2009)
Golfier, F., Quintard, M., Cherblanc, F., Zinn, B.A., Wood, B.D.: Comparison of theory and experiment for solute transport in highly heterogeneous porous medium. Adv. Water Resour. **30**, 2235–2261 (2007)
Gray, W.G.: A derivation of the equations for multi-phase transport. Chem. Eng. Sci. **30**, 229–233 (1975)
Kaviany, M.: Principles of Convective Heat Transfer, Principles of Heat Transfer in Porous Media. Springer, New York (1991)
Kim, J.H., Ochoa, J.A., Whitaker, S.: Diffusion in anisotropic porous media. Transp. Porous Media **2**, 327–356 (1987)
Lux, J.: A non-periodic closure scheme for the determination of effective diffusivity in real porous media. Transp. Porous Media **82**, 299–315 (2010)
Marle, C.M.: Application de la mthode de la thermodynamique des processus irrversibles lcoulement dun fluide travers un milieux poreux. Bull. RILEM **29**, 1066–1071 (1965)
Marle, C.M.: Ecoulements monophasiques en milieu poreux. Revue de lInstitut Franaise du Pétrole **22**, 14711509 (1967)
Marle, C.M.: On macroscopic equations governing multiphase flow with diffusion and chemical reactions in porous media. Int. J. Eng. Sci. **20**, 643–662 (1982)
Matheron, G.: Les Variables régionalisées et leur estimation. Masson, Paris (1965)
Mls, J.: On the existence of the derivative of the volume average. Transp. Porous Media **2**, 615–621 (1987)
Moyne, C.: Two-Equation model for a diffusion process in porous media using the volume averaging method with an unsteady closure. Adv. Water Resour. **20**, 63–76 (1997)
Moyne, C., Didierjean, S., Amaral Souto, H.P., Da Silveira, O.T.: Thermal dispersion in porous media: one-equation model. Int. J. Heat Mass Transf. **43**, 3853–3867 (2000)
Mukasyan, A.S., Rogachev, A.S.: Discrete reaction waves: gasless combustion of solid powder mixtures. Prog. Energy Combust. Sci. **34**, 377–416 (2008)
Nozad, I., Carbonell, R.G., Whitaker, S.: Heat conduction in multiphase systemsI: theory and experiment for two-phase systems. Chem. Eng. Sci. **40**, 843–855 (1985)
Ochoa, J.A., Stroeve, P., Whitaker, S.: Diffusion and reaction in cellular media. Chem. Eng. Sci. **41**, 2999–3013 (1986)
Prat, M.: On the boundary conditions at the macroscopic level. Transp. Porous Media **4**, 259–280 (1989)
Puiroux, N., Prat, M., Quintard, M.: Non-equilibrium theories for macroscale heat transfer: ablative composite layer systems. Int. J. Thermal Sci. **43**, 541–554 (2004)
Quintard, M.: Diffusion in isotropic and anisotropic porous systems: three-dimensional calculations. Transp. Porous Media **11**, 187–199 (1993)
Quintard, M., Whitaker, S.: One-and two-equation models for transient diffusion processes in two-phase systems. Adv. Heat Transf. **23**, 369–464 (1993)
Quintard, M., Whitaker, S.: Transport in ordered and disordered porous media I: the cellular average and the use of weighting functions. Transp. Porous Media **14**, 163–177 (1994a)
Quintard, M., Whitaker, S.: Transport in ordered and disordered porous media II: generalized volume averaging. Transp. Porous Media **14**, 179–206 (1994b)
Quintard, M., Whitaker, S.: Transport in ordered and disordered porous media III: closure and comparison between theory and experiment. Transp. Porous Media **15**, 31–49 (1994c)
Quintard, M., Whitaker, S.: Theoretical analysis of transport in porous media. Handbook of Heat Transfer in Porous Media, pp. 1–52 (2000)

Quintard, M., Cherblanc, F., Whitaker, S.: Dispersion in heterogeneous porous media: one-equation non-equilibrium model. Transp. Porous Media **44**, 181–203 (2001)
Quintard, M., Kaviany, M., Whitaker, S.: Two-medium treatment of heat transfer in porous media: numerical results for effective properties. Adv. Water Resour. **20**, 77–94 (1997)
Quintard, M., Ladevie, B., Whitaker, S.: Effect of homogeneous and heterogeneous source terms on the macroscopic description of heat transfer in porous media. In: Symposium on Energy Engineering in the 21st Century 2, pp. 482–489 (2000)
Ryan, D.: Effective diffusivities in reactive porous media: a comparison between theory and experiments. Master's Thesis, UC Davis (1983)
Ryan, D., Carbonell, R.G., Whitaker, S.: A theory of diffusion and reaction in porous media. AIChE Symp. Ser. **77**, 46–62 (1981)
Sanchez-Palencia, E.: Lecture Notes in Physics, vol 127: Nonhomogeneous Media and Vibration Theory. Springer, New York (1980)
Sahraoui, M., Kaviany, M.: Direct simulation versus local, phase-volume averaged description of adiabatic premixed flame in a porous medium. Int. J. Heat Mass Transf. **37**, 2817–2834 (1994)
Shapiro, M., Brenner, H.: Taylor dispersion of chemically reactive species: irreversible first-order reactions in bulk and on boundaries. Chem. Eng. Sci. **41**, 1417–1433 (1986)
Shapiro, M., Brenner, H.: Dispersion of a chemically reactive solute in a spatially periodic model of a porous medium. Chem. Eng. Sci. **43**, 551–571 (1988)
Shonnard, D.R., Whitaker, S.: The effective thermal conductivity for a point-contact porous medium: an experimental study. Int. J. Heat Mass Transf. **32**, 503–512 (1989)
Slattery, J.C.: Flow of viscoelastic fluids through porous media. AIChE J. **13**, 1066–1071 (1967)
Valdés-Parada, F.J., Aguilar-Madera, C.G.: Upscaling mass transport with homogeneous and heterogeneous reaction in porous media. Chem. Eng. **24**, 1453 (2011)
Valdés-Parada, F.J., Alvarez-Ramirez, J.: On the effective diffusivity under chemical reaction in porous media. Chem. Eng. Sci. **65**, 41004104 (2010)
Vandadi, V., Park, C., Kaviany, M.: Superadiabatic radiant porous burner with preheater and radiation corridors. Int. J. Heat Mass Transf. **64**, 680–688 (2013)
Whitaker, S.: Diffusion and dispersion in porous media. AIChE J. **13**, 420427 (1967)
Whitaker, S.: Simultaneous heat, mass, and momentum transfer in porous media: a theory of drying. Adv. Heat Transf. **13**, 119–203 (1977)
Whitaker, S.: Mass transport and reaction in catalyst pellets. Transp. Porous Media **2**, 269–299 (1987)
Whitaker, S.: The Method of Volume Averaging. Springer, New York (1999)